

A statistical study of nearby galaxies

I: NIR growth curves and optical-to-NIR colors as a function of type, luminosity and inclination

Michel Fioc^{1,2} and Brigitte Rocca-Volmerange^{2,3}

¹ NASA/Goddard Space Flight Center, code 685, Greenbelt, MD 20771, USA

² Institut d'Astrophysique de Paris, CNRS, 98 bis Bd Arago, F-75014 Paris, France

³ Institut d'Astrophysique Spatiale, Bât. 121, Université Paris XI, F-91405 Orsay, France

Received / Accepted

Abstract. Growth curves of the near-infrared (NIR) magnitude as a function of the aperture have been built and used to derive NIR total magnitudes from aperture data taken from the literature. By cross-correlating with optical and redshift data, absolute magnitudes and optical-to-NIR colors have been computed for some 1000 galaxies of different types. Significant color gradients are observed, underlining that small aperture colors may lead to a biased picture of the stellar populations of galaxies.

A statistical analysis using various estimators taking into account the intrinsic scatter has been performed to establish relations between the colors, the morphological type, the inclination or the shape, and the intrinsic luminosity.

The combination of the optical and the NIR should obviously improve our understanding of the evolution of galaxies. Despite the intrinsic scatter, especially among star-forming galaxies, optical-to-NIR colors show a very well defined sequence with type, blueing by 1.3 mag from ellipticals to irregulars. The colors of spiral galaxies strongly redden with increasing inclination and put new constraints on the modeling of the extinction. No such effect is observed for lenticular galaxies. We also find that rounder ellipticals tend to be redder.

A color-absolute magnitude relation is observed inside each type, with a slope significantly steeper for early and intermediate spirals than for ellipticals or late spirals. This stresses the importance of considering both the mass and the type to study the star formation history of galaxies.

Key words: Galaxies: evolution – Galaxies: fundamental parameters – Galaxies: photometry – Galaxies: statistics – Infrared: galaxies – dust, extinction

1. Introduction

Although color-magnitude diagrams have now been obtained for a few very close galaxies – most of them dwarf –, allowing to study directly their stellar populations (e.g. Schulte-Ladbeck & Hopp 1998; Aparicio 1998), the synthesis of the spectral energy distribution (SED) of nearby galaxies remains the most efficient and systematic method to trace their star formation history up to $z = 0$.

Early optical studies have shown a clear correlation between the SED – and hence the star formation history – and the galaxy Hubble type. However, the age-star formation timescale and age-metallicity degeneracies make it highly desirable to extend the wavelength range to the ultraviolet (UV) and the near-infrared. Whereas the ultraviolet is related to the young stellar populations in currently star-forming galaxies, the near-infrared is dominated by old giant stars and is a measure of the star formation rate integrated from the beginning, i.e. of the stellar mass of the galaxy. When compared to shorter wavelengths, the NIR may moreover put constraints on the stellar metallicity, owing to the high sensitivity of the effective temperature of red giants to the abundance of heavy elements. In combination with optical data, it finally provides clues on the amount and the distribution of dust because of the different extinction at both wavelengths.

Observations in the UV and the NIR are however hampered by the atmosphere. Though interesting to study the detailed star formation history of a specific galaxy, the spectra obtained from Space are too scarce to afford a statistical analysis from which the general trends as a function of type or mass, or the effect of the dust, may be derived. In spite of the loss of spectral resolution, broad-band colors in the J , H and K atmospheric windows are more promising. As the spectra, they are usually obtained in small apertures not representative of the whole galaxy because of the color gradients, especially for disk galaxies, and have to be extrapolated to be compared to the optical data. Such extrapolation is however much easier for

colors than for spectra and can be applied to hundreds of objects.

In the following, we analyze a catalog of infrared aperture magnitudes (section 2) and combine it with optical catalogs to derive NIR growth curves of the magnitude as a function of the aperture (section 3). We then compute total and effective magnitudes and colors (section 4). The NIR and optical-to-NIR colors are analyzed statistically as a function of type, luminosity and inclination in section 5. We finally discuss our results in section 6.

2. The optical and infrared data

The near-infrared data used in this paper come from the CIO catalog (Gezari et al. 1997) which is a compilation of the NIR observations published before 1995. They are given in a large variety of systems (magnitudes m_λ , F_λ , F_ν , etc.) and units, and are first converted to magnitudes assuming Vega has a magnitude of 0.03. The data are reduced from the wavelength λ to the central wavelengths of the J ($\lambda_J = 1.24\mu\text{m}$), H ($\lambda_H = 1.65\mu\text{m}$) and K ($\lambda_K = 2.21\mu\text{m}$) filters of Bessel & Brett (1988), assuming the following color equations:

$$\begin{aligned} m_J &= m_\lambda + (\lambda_J - \lambda) \frac{< J - H >}{\lambda_J - \lambda_H}, \\ m_H &= m_\lambda + (\lambda_H - \lambda) \frac{< J - H >}{\lambda_J - \lambda_H} && \text{if } \lambda < 1.65\mu\text{m}, \\ &= m_\lambda + (\lambda_H - \lambda) \frac{< H - K >}{\lambda_H - \lambda_K} && \text{if } \lambda > 1.65\mu\text{m}, \\ m_K &= m_\lambda + (\lambda_K - \lambda) \frac{< H - K >}{\lambda_H - \lambda_K}, \end{aligned}$$

where $< J - H > = 0.7$ and $< H - K > = 0.2$ are the typical $J - H$ and $H - K$ colors of a normal galaxy and depend very little on the galaxy type or the aperture.

The CIO catalog is cross-correlated with the RC3 catalog (de Vaucouleurs et al. 1991) to correct for the Galactic extinction. The NIR extinction is computed from A_B as follows: $A_J = 0.182A_B$, $A_H = 0.098A_B$, $A_K = 0.068A_B$.

The magnitudes are also corrected for the redshift z as $m_\lambda(0) = m_\lambda(z) - k_\lambda(z)$. Values of $k_\lambda(z)$ are given in Table 1 for different types of galaxies and have been computed using the PÉGASE model of spectral evolution (Fioc & Rocca-Volmerange 1997). They should be used only at $z < 0.1$. The redshift is taken from the NED database. For a few galaxies, z is unknown and we compute the k -correction (but not the absolute magnitudes) assuming $z = 0.01$, the mean redshift of our catalog.

The RC3 provides us also with the morphological type T , the ratio R_{25} of the major axis (D_{25}) to the minor axis of the ellipsis corresponding to the isophot $\mu = 25\text{mag/arcsec}^2$, the total B -magnitude B_T extrapolated to an infinite radius and the circular effective aperture A_e containing half the light emitted in the B -band.

type	k_B	k_J	k_H	k_K
E	5.1z	-0.3z	-0.1z	-2.8z
S0	4.9z	-0.3z	-0.1z	-2.8z
Sa	4.0z	-0.3z	-0.1z	-2.8z
Sb	3.6z	-0.3z	-0.1z	-2.8z
Sc	2.6z	-0.3z	-0.1z	-2.8z
Sd	2.2z	-0.5z	-0.3z	-2.8z
Im	1.8z	-0.7z	-0.4z	-2.8z

Table 1. k -corrections in B , J , H and K as a function of the type.

When available, we prefer to take B_T and A_e from the more recent catalog Hypercat (Prugniel & Héraudeau 1998). This catalog also gives the photometric type T_p corresponding to the best-fitting growth curve $\mathcal{B}(X, T_p)$ of the B -magnitude as a function of the circular aperture A , where $X = \log_{10}(A/A_e)$ (see Appendix A).

3. The NIR growth curve

The detailed 2D-fitting of the profile of galaxies (de Jong & van der Kruit 1994) is certainly the best way to compute their total magnitudes, but surface photometry in the NIR is available for too few of them to perform a statistical analysis. The largest such study is based on only 86 spiral galaxies of all types (de Jong 1996a, 1996b, 1996c), to compare to typically 100 galaxies *per type* in this paper. We therefore prefer to extrapolate aperture magnitudes with a growth curve. The computation of total (i.e. asymptotic) NIR magnitudes comparable to the optical ones determined by, e.g., de Vaucouleurs et al. (1991) or Prugniel & Héraudeau (1998) is however made difficult by the small apertures achieved at these wavelengths. Few galaxies have enough data from small to large apertures to constrain the shape of the growth curve and one has to use another method, combining observations of different galaxies having presumably the same curve (cf. Griersmith 1980). To this purpose, one needs to scale the apertures to a characteristic length A_c for each galaxy. The NIR growth curve $\mathcal{M}(A/A_c)$ is then built by plotting $m(A) - m(A_c)$ as a function of $\log_{10}(A/A_c)$. Usually (Gavazzi et al. 1996a; Gavazzi & Boselli 1996; Tormen & Burstein 1995; Frogel et al. 1978; Aaronson et al. 1979), the D_{25} diameter has been used as characteristic length. As noticed however by de Vaucouleurs et al. (1976), the D_{25} diameter depends not only on the shape of the profile but also on the central surface brightness. For this reason, the ratio of the effective aperture A_e to D_{25} is not a constant.

We prefer to adopt here an other procedure. We may expect some relation between the optical profile and the NIR profile. For this reason, we decide to build a growth curve as a function of the B photometric type T_p taken from Hypercat and of $X = \log_{10}(A/A_e)$. The infrared magnitude $m(A_e)$ in the B effective aperture is computed

by interpolation or by a small extrapolation in $\log_{10}(A)$. Rather than a straight line, we have used the functions proposed to compute H magnitudes at $A = D_{25}$ by Gavazzi et al. (1996a):

$$\mathcal{M}(X_{25}) = a + b(-0.35X_{25} + 1.68X_{25}^2 + 0.07X_{25}^3)$$

where $X_{25} = \log_{10}(A/D_{25})$, and fitted a and b to the observations. This takes into account the curvature of the growth curve near A_e and improves the determination of $m(A_e)$. Because they are polynomials, these functions are however not suitable to extrapolate the magnitude to the infinity.

The J , H and K data have been combined to build the growth curve. This is justified by the fact that only small $J - H$ and $H - K$ color gradients are observed (Aaronson 1977; Frogel et al. 1978). The growth curves are plotted in Fig. 1 for 7 bins of photometric type. As evidenced by this graph, the NIR growth curve is flatter than the optical one, especially for T_p corresponding to intermediate spirals: the NIR emission of galaxies is more concentrated than in the optical. This behavior is expected because the bulge is redder than the disk and is therefore more prominent in the NIR than in the optical. The scatter is also higher for intermediate types, which might be due to an inclination dependency of the growth curve (Christensen 1990; Kodaira et al. 1990). We have therefore distinguished in Fig. 1 between galaxies with $R_{25} < 0.3$ (rather face-on for disk galaxies) and $R_{25} > 0.3$, but no obvious trend is observed and we will neglect any inclination dependency in the following.

Because of the scatter and the lack of data at high aperture, where the flattening of the growth curve puts constraints on the curvature, attempts to fit growth curves similar to those of Prugniel & Héraudeau (1998) with 3 parameters (m_T , $\log_{10}(A_e)$ and T_p) did not prove successful. Plotting the NIR magnitudes versus the B magnitudes however reveals a nearly linear – though scattered – relation, between these quantities, suggesting to adopt a NIR growth curve of this form:

$$\mathcal{M}(X, T_p) = s\mathcal{B}(X, T_p).$$

This ensures that the extrapolation at infinite A converges since $\lim_{X \rightarrow \infty} \mathcal{B}(X, T_p) = 0$. Such relation has been fitted for each photometric type bin (Fig. 1, dashed lines) at $X > -1.5$.

The dispersion is due both to the uncertainties in the individual data and to the intrinsic scatter in the shape of the NIR growth curves for a given B photometric type. The following convention is adopted hereafter: $x \sim \mathcal{N}(\mu, \sigma^2)$ means that x is distributed according to (or the density probability of x is) a Gaussian with mean μ and variance σ^2 . Let us assume that, for each galaxy, the distribution of individual data around the best-fitting NIR growth curve $s\mathcal{B}(X, T_p)$ is $\sim \mathcal{N}(0, \sigma_{m_0}^2)$ and that the distribution of the parameter s characterizing the growth

curve is $s \sim \mathcal{N}(s_0, \sigma_{s_0}^2)$. At any aperture,

$$m(X) - m(0) \sim \mathcal{N}\left\{s_0[\mathcal{B}(X, T_p) - \mathcal{B}(0, T_p)], \sigma_{m_0}^2 + \sigma_{s_0}^2 [\mathcal{B}(X, T_p) - \mathcal{B}(0, T_p)]^2\right\}.$$

A maximum likelihood estimation of these parameters yields $\sigma_{m_0} \simeq 0.06$, nearly independent of T_p , $\sigma_{s_0} \simeq 0.10$ for early types ($T_p < -1$) and $\sigma_{s_0} \simeq 0.15$ at later types. The value of s_0 we obtained is plotted as a function of the median T_p of each bin in Fig. 1 and may be approximated with the following formulae:

$$\begin{aligned} s_0 &= 0.87 & \text{if } T_p < -4.5, \\ &= 0.74 - 0.029T_p & \text{if } -4.5 < T_p < 2.5, \\ &= 0.64 + 0.011T_p & \text{if } T_p > 2.5. \end{aligned}$$

The mean value s_0 is less than one for all types, corresponding as expected to a blue-outwards gradient. This gradient is low for early-types, increases for spirals, peaking at $T_p \in [2-4]$ (\sim Sb) in good agreement with what has been obtained at optical wavelengths by de Vaucouleurs & Corwin (1977) and remains constant or slightly decreases for late types. The typical blueing of the $B -$ NIR color of spirals from the effective aperture to the infinity is $-0.75(1 - s) \sim -0.2$, close to the median value (-0.19) in $B - H$ and $B - K$ we have computed from the profiles published by de Jong (1996a).

4. Effective and total near-infrared magnitudes

4.1. Apparent magnitudes and colors

Effective and total near-infrared magnitudes have been computed for all the galaxies with known effective aperture by fitting the growth curves $s\mathcal{B}(X, T_p)$ introduced in the previous section to the observed data (X_i, m_i, σ_i) , $i \in [1, n]$, where σ_i is the uncertainty on the magnitude m_i . The asymptotic magnitude depends primarily on the shape of the growth curve at large aperture. To avoid problems with small apertures suffering from seeing or off-centering, or which are contaminated by nuclear emission or a central starburst, we remove all the observations at $X < -1$ from the fit.

The procedure to compute the total and effective NIR magnitudes m_T , m_e and the corresponding uncertainties $\sigma(m_T)$, $\sigma(m_e)$ due to the uncertainties in the aperture magnitudes is detailed in Appendix B.

The global uncertainty ς_{m_T} on m_T taking also into account the uncertainties in T_p and A_e is finally computed from

$$\varsigma_{m_T}^2 = \sigma^2(m_T) + \left(\frac{\partial m_T}{\partial T_p}\right)^2 \sigma^2(T_p) + \left(\frac{\partial m_T}{\partial A_e}\right)^2 \sigma^2(A_e)$$

and the same for ς_{m_e} .

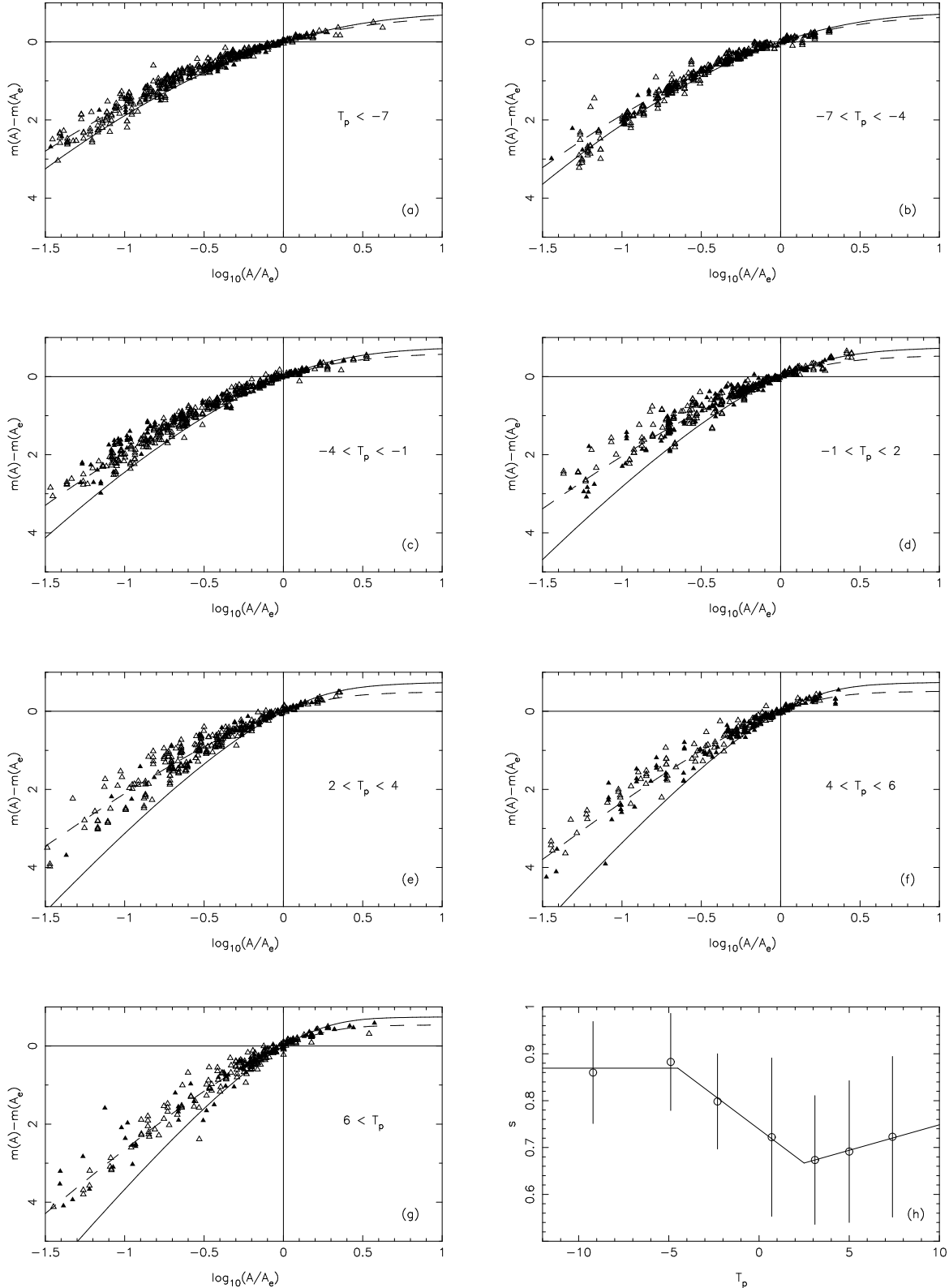


Fig. 1. (a) to (g): Growth curve of the NIR magnitude as a function of the aperture for the different photometric types. Hollow and filled triangles correspond respectively to galaxies with $\log_{10} R_{25} < 0.3$ and $\log_{10} R_{25} > 0.3$. The solid and dashed lines are the mean optical and NIR growth curves. They are normalized to the effective aperture in the B -band and to the corresponding magnitude. **(h):** The circles and vertical segments are the mean value s_0 and the intrinsic scatter σ_{s_0} of s as a function of the median value of T_p in each bin. The broken line is the 3-slope fit to $s_0(T_p)$ given in the text.

In many cases, the photometric type is unknown and we estimate it from the morphological type with the following relations derived by cross-correlating Hypercat and the RC3:

$$\begin{aligned} T_p &= -2.3 + 0.5T & \text{if } T < -1, \\ &= -1.32 + 1.48T & \text{if } -1 < T < 4, \\ &= 1.4 + 0.8T & \text{if } T > 4. \end{aligned}$$

We then simply assume $\sigma(T_p) = 3$.

The uncertainty on the colors $m_1 - m_2$, where $(m_1, m_2) \in [J, H, K]^2$, is computed as

$$\begin{aligned} \varsigma_{m_1 - m_2}^2 &= \sigma^2(m_1) + \sigma^2(m_2) + \left[\frac{\partial(m_1 - m_2)}{\partial T_p} \right]^2 \sigma^2(T_p) \\ &\quad + \left[\frac{\partial(m_1 - m_2)}{\partial A_e} \right]^2 \sigma^2(A_e). \end{aligned}$$

However, this is clearly an overestimate because J , H and K data have usually been observed simultaneously and their errors are presumably highly positively correlated.

When B is one of the band, e.g. $m_1 = B_T$, the partial derivatives are unknown. We then estimate $\varsigma_{m_1 - m_2}$ as

$$\varsigma_{m_1 - m_2}^2 = \varsigma_{m_1}^2 + \varsigma_{m_2}^2.$$

This will usually be a slight overestimate for the partial derivatives of B_T and m_2 should have the same sign, but most of the uncertainty comes actually from the NIR data themselves.

4.2. Absolute magnitudes

The absolute magnitude M_T is computed as

$$M_T = m_T - 25 - 5 \log_{10}(v_V/H_0)$$

where v_V is the velocity of a galaxy derived from the redshift z and corrected for the movement of the Sun in the restframe of the Virgo cluster according to the equations (18), (19), (20), (31) and (32) from Paturel et al. (1997). We assume $H_0 = 65 \text{ km.s}^{-1} \text{ Mpc}^{-1}$. The uncertainty on the absolute magnitude is computed from

$$\varsigma_{M_T}^2 = \varsigma_{m_T}^2 + \left[\frac{5}{\ln(10)} \right]^2 \frac{(\partial v_V / \partial z)^2 \sigma^2(z) + v_p^2}{v_V^2}$$

where $v_p = 350 \text{ km.s}^{-1}$ is the typical peculiar velocity of galaxies in the Las Campanas Redshift Survey (Lin et al. 1996). At low redshift, peculiar velocities perturb the redshift-distance relation and increase the uncertainty on the absolute magnitude. All the absolute magnitudes of the galaxies with $[(\partial v_V / \partial z)^2 \sigma^2(z) + v_p^2]^{1/2} > v_V/3$ have been discarded in the following. $\sigma(z)$ has been computed according to the formulae (1) and (2) of the Appendix A of Paturel et al. (1997), taking into account both the internal uncertainty on the values of the redshift and the discrepancies between them.

Covariances between the colors and the absolute magnitudes have also been computed.

type	T (RC3)
E	$T < -3.5$
S0	$-3.5 < T < -0.5$
Sa	$-0.5 < T < 1.5$
Sb	$1.5 < T < 3.5$
Sbc	$3.5 < T < 4.5$
Sc	$4.5 < T < 5.5$
Sd	$5.5 < T < 8.5$
Im	$8.5 < T$

Table 2. Correspondence between the types used in this paper and the RC3 types.

5. Statistics of optical-near infrared colors

5.1. $J - H$, $H - K$ and $J - K$ colors

The galaxies have been distributed in eight broad types according to the morphological type T taken from the RC3 (see Table 2). The $J - H$, $H - K$ and $J - K$ total and effective colors have been plotted in figure 2 as a function of the type.

Because the uncertainties computed for $J - H$, $H - K$ and $J - K$ are overestimates, we simply give in table 3 the median color for each type and compute its uncertainty by a bootstrap with replacement. The total and effective colors show almost no difference. Whereas $H - K$ seems to be nearly independent of the type, $J - H$ and $J - K$ decrease clearly at the late types, indicating that the J -band is contaminated by young stars. The colors are also redder for early-type spirals, which is difficult to understand with current models of stellar evolution and atmospheres. This effect is observed in both the total and effective colors. The extrapolation to compute the latter being small, this may not come from a problem with the growth curve. The extinction, negligible in the NIR, is also unlikely to cause this phenomenon. A possible explanation is that we begin to see in H and K the tail of the dust infrared emission at short wavelengths. We note in particular that the J and K samples contain a non-negligible fraction of galaxies with nuclear activity of which central colors are in some cases as red as $J - H \sim H - K \sim 1$.

5.2. $B - J$, $B - H$ and $B - K$ colors

The catalog is large enough to perform a statistical analysis of the colors as a function of the type, the luminosity and the inclination or the shape (R_{25}) of the galaxy. An interesting quantity is also the intrinsic scatter in the colors at a given type, luminosity and R_{25} , for it is a measure of the variations of the star formation history and of the effects of dust (e.g. Peletier & de Grijs 1998; Shioya & Bekki 1998). Note however that the intrinsic scatter may depend on the type-binning, especially if the colors evolve rapidly from type to type.

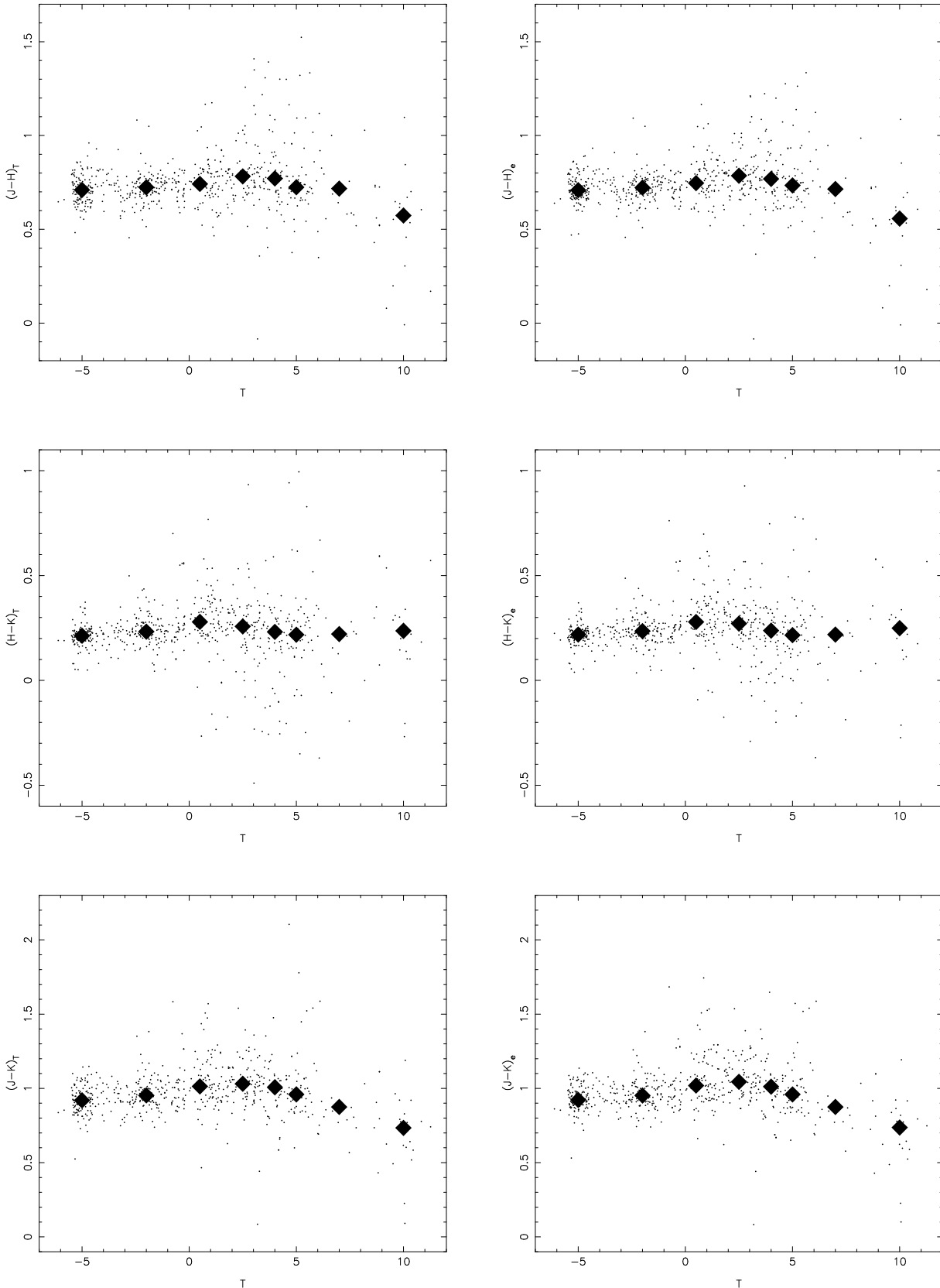


Fig. 2. Total and effective NIR colors as a function of type. A random component in $[-0.5, 0.5]$ has been added to the type to make the graph clearer. The diamonds are the median colors per type.

type	N	$(J - H)_T$ median	$(J - H)_e$ median	N	$(H - K)_T$ median	$(H - K)_e$ median	N	$(J - K)_T$ median	$(J - K)_e$ median
E	140	0.71 ± 0.01	0.71 ± 0.01	141	0.21 ± 0.01	0.22 ± 0.01	140	0.92 ± 0.01	0.92 ± 0.01
S0	154	0.72 ± 0.01	0.72 ± 0.01	157	0.23 ± 0.01	0.23 ± 0.01	155	0.95 ± 0.01	0.95 ± 0.01
Sa	96	0.74 ± 0.01	0.75 ± 0.01	96	0.28 ± 0.01	0.28 ± 0.01	97	1.01 ± 0.01	1.02 ± 0.01
Sb	93	0.78 ± 0.01	0.79 ± 0.01	95	0.26 ± 0.01	0.27 ± 0.01	95	1.03 ± 0.01	1.04 ± 0.01
Sbc	46	0.77 ± 0.02	0.77 ± 0.02	47	0.23 ± 0.02	0.24 ± 0.02	47	1.01 ± 0.02	1.01 ± 0.01
Sc	46	0.72 ± 0.02	0.73 ± 0.02	46	0.22 ± 0.02	0.22 ± 0.02	46	0.96 ± 0.02	0.96 ± 0.02
Sd	26	0.72 ± 0.04	0.71 ± 0.04	24	0.22 ± 0.04	0.22 ± 0.04	24	0.87 ± 0.05	0.88 ± 0.04
Im	22	0.57 ± 0.05	0.56 ± 0.03	20	0.24 ± 0.05	0.25 ± 0.04	25	0.73 ± 0.05	0.74 ± 0.06

Table 3. Median total and effective $J - H$, $H - K$ and $J - K$ colors (with their 1σ -uncertainties) as a function of type.

The $B - H$ sample is by far the largest (more than 900 galaxies in $B - H$ against 600 in $B - J$ and $B - K$). It is also the most accurate (the uncertainty is typically 0.16 mag in $(B - H)_T$ and 0.09 mag in $(B - H)_e$) and the most complete in type, whereas the $B - J$ and $B - K$ sample are strongly deficient in the latest types. For these various reasons, we will mainly focus our discussion in the following on the analysis of the $B - H$ data.

We adopt here the formalism proposed by Akritas (1999). Let us assume that the true color Y_i of the i^{th} galaxy depends linearly on p quantities $X_{ij}, j \in [1, p]$ (the X_{ij} being, e.g., $\log_{10}(R_{25})$ or the absolute magnitude):

$$Y_i = \beta_0 + \sum_{j=1}^p \beta_j (X_{ij} - \mu_j) + \epsilon_i,$$

where μ_j , the median of X_{ij} , is introduced merely to identify β_0 with the typical color of the sample, and ϵ_i is the deviation from the relation due to the intrinsic scatter. We assume that $\epsilon_i \sim \mathcal{N}(0, \sigma^2)$ independently of the other parameters. Let us write $\beta_{p+1} = \sigma$ to remind that the scatter is also to be determined.

The observed variables, x_{ij} and y_i , are related to the true variables by

$$x_{ij} = X_{ij} + \epsilon_{ij},$$

$$y_i = Y_i + \epsilon_{Yi},$$

where $\epsilon_{ij} \sim \mathcal{N}(0, \sigma_{ij}^2)$ and $\epsilon_{Yi} \sim \mathcal{N}(0, \sigma_{Yi}^2)$. We obtain

$$y_i - \beta_0 - \sum_{j=1}^p \beta_j (x_{ij} - \mu_j) = \epsilon_{Yi} - \sum_{j=1}^p \beta_j \epsilon_{ij} + \epsilon_i.$$

Assuming that ϵ_i is not correlated with the ϵ_{ij} and ϵ_{Yi} , and that the covariances between ϵ_{ij} and ϵ_{ik} and between ϵ_{ij} and ϵ_{ijY} are γ_{ijk} and γ_{ijY} , respectively, we obtain that $y_i - \beta_0 - \sum_{j=1}^p \beta_j (x_{ij} - \mu_j) \sim \mathcal{N}(0, \sigma_i^2 + \beta_{p+1}^2)$ with

$$\sigma_i^2 = \sigma_{Yi}^2 + \sum_{j=1}^p \beta_j^2 \sigma_{ij}^2 - 2 \sum_{j=1}^p \beta_j \gamma_{ijY} - \sum_{j,k=1}^p \beta_j \beta_k \gamma_{ijk}.$$

We have tested two procedures to estimate the β_j from our sample. The first one estimates the β_j by maximizing the logarithm of the likelihood Λ with respect to the $\beta_j, j \in [0, p+1]$, where

$$\ln(\Lambda) = -\frac{1}{2} \sum_{i=1}^n \left\{ \frac{[y_i - \beta_0 - \sum_{j=1}^p \beta_j (x_{ij} - \mu_j)]^2}{\sigma_i^2 + \beta_{p+1}^2} + \ln(\sigma_i^2 + \beta_{p+1}^2) \right\}$$

according to the formulae given above. The covariance matrix of the β_j is computed by inverting the curvature matrix (α_{ij}) , $(i, j) \in [0, p+1]^2$, where

$$\alpha_{ij} = \frac{\partial^2 [-\ln(\Lambda)]}{\partial \beta_i \partial \beta_j} \quad (\text{Kendall \& Stuart 1979}).$$

Maximum likelihood (ML) estimators are often biased and we therefore wish to compare to another method.

The second procedure (MCES estimators) has been developed by Akritas & Bershady (1996) and Akritas (1999). According to the authors, it yields unbiased estimators. However, the σ_{Yi} are not used in the expression of the $\beta_i, i \leq p$, which means that they have all the same weight. This is especially not satisfying if the intrinsic scatter is small or comparable to the uncertainties in the colors – which happens in particular for elliptical galaxies – and may give an excessive importance to outliers. The authors also do not provide the intrinsic scatter β_{p+1} and we estimate it from

$$\beta_{p+1}^2 = \frac{1}{n} \sum_{i=1}^n \left\{ [y_i - \beta_0 - \sum_{j=1}^p \beta_j (x_{ij} - \mu_j)]^2 - \sigma_i^2 \right\}$$

but when the intrinsic scatter is smaller or of the same order than the uncertainties in the observables, it is underestimated¹ and we may even obtain a negative (and

¹ This is shown by the fact that the ML and MCES estimators of the scatter in the effective colors (which are less uncertain) are similar and are also close to the ML estimator for the total colors, whereas the MCES intrinsic scatter in the total colors is smaller.

meaningless) value. We then assume $\beta_{p+1} = 0$. Uncertainties on the β_j have been computed by a bootstrap with replacement on the (x_{ij}, y_i) rather than by using the cumbersome formulae proposed by Akritas & Bershady (1996) and Akritas (1999), which anyway are not available for β_{p+1} .

Note that the uncertainties determined either from the curvature matrix or by bootstrap become themselves very uncertain when the number of galaxies is less than about 20 to 30.

In the following, values determined by the ML and MCES estimators are written in boldface and italic characters, respectively.

Because we are mainly interested in “normal” galaxies, we have to reject a few galaxies with unusual colors (Buta et al. 1994). Most of them are extremely blue and, according to their optical colors (when available), are presumably starbursting galaxies. Some blue compact dwarfs may also be misclassified from their morphology as ellipticals. In the opposite, our sample contains some galaxies with very red colors, especially in the K -band and their NIR emission is dominated by an active nucleus. To reject these galaxies, we apply an iterative method. Rather than using the standard deviation around the best fit, which is very sensitive to the outliers, we estimate the observational scatter from the median of the absolute deviations. At each step, we compute

$$\delta = 1.48 \operatorname{median}_{i \in [1, n]} \left| y_i - \beta_0 - \sum_{j=1}^p \beta_j (x_{ij} - \mu_j) \right|$$

from the sample (including the “abnormal” galaxies), the factor 1.48 ensuring that in the case of a perfectly Gaussian distribution, the standard deviation is δ ; we define “normal” galaxies as those having $\left| y_i - \beta_0 - \sum_{j=1}^p \beta_j (x_{ij} - \mu_j) \right| < 3\delta$ and then determine the β_j from them only by either of the methods discussed above. We iterate this procedure 4 times, but the convergence is usually achieved at the third one.

5.3. The type-color relation

The total and effective $B - J$, $B - H$ and $B - K$ colors have been plotted as a function of the morphological type on Figure 3. A very impressive trend to bluer colors with advancing type is observed. The mean $(B - H)_T$ of irregular galaxies is 1.34 mag bluer than the one of ellipticals, to be compared to 0.68 in $U - B$, 0.47 in $B - V$, 0.46 in $V - I_c$ and only 0.23 in $V - R_c$ (Fioc & Rocca-Volmerange, in preparation). A similar gap between the $(B - H)_T$ of ellipticals and irregulars was obtained in $(B - H)_e$ by Buta (1995) from a sample of 225 galaxies.

The $(B - H)_T$ colors determined by the ML estimator are almost always systematically redder by ~ 0.02 mag than those computed using the MCES estimator. This bias comes from the fact that the uncertainties are smaller for

brighter galaxies in the NIR, which are also usually redder. The ML estimator giving more weight to the data with smaller uncertainties, it is biased to the red.

A significant scatter is also observed within each type. Part of it is due to the observational uncertainties, but it comes mainly from the *intrinsic* scatter in the colors. The intrinsic scatter increases from **0.13/0.08**, depending on the estimator, for ellipticals to ~ 0.4 for Sb and remains nearly constant at later types.

5.4. The R_{25} -color relation

The color-inclination relation is potentially a very powerful constraint on the amount of dust and its distribution relatively to stars. As a disk becomes more and more inclined, its optical depth increases and the colors redden. This must be especially striking when one of the band (e.g. B) is heavily extinguished whereas the dust is almost transparent in the other one (e.g. H). For these reasons, various studies have tried to determine a color-inclination relation, regrouping the galaxies either as a function of type (e.g. Boselli & Gavazzi 1994) or as a function of their NIR absolute magnitude (Tully et al. 1998). The samples used in these studies were however small (about 100 galaxies) and it is worth to look at the relation once again with our much larger catalog.

For an oblate ellipsoid, which is a standard model for a galaxy disk (Hubble 1926), the inclination i (face-on corresponds to $i = 0$) is related to the true ratio q_0 of the minor to the major axis and to the apparent ratio $q \simeq 1/R_{25}$ by

$$\cos^2 i = \frac{q^2 - q_0^2}{1 - q_0^2}.$$

Practically, we prefer to establish a relation between the colors and $\log_{10}(R_{25})$, both because R_{25} is the directly observed quantity and because the linear estimators used here provide a better fit when $\log_{10}(R_{25})$ is used rather than i or $\cos(i)$.

The relations are plotted in Fig. 4 and statistical estimators of the slope and the color are given in table 7 for $B - H$. The slopes are represented as a function of type in figure 5. Also shown on this graph are the slopes derived from the larger $B - V$ and $U - B$ samples.

The typical slope of the $(B - H)_T$ - $\log_{10}(R_{25})$ relation is about 1 for spiral galaxies, to be compared to 0.2–0.3 in $B - V$ and $U - B$.

Surprisingly high is the value of the slope for Sa galaxies. However, the slope of the $(B - H)_T$ -*inclination* relation would be shallower for Sa since q_0 is a decreasing function of type (Bottinelli et al. 1983), i.e. Sa galaxies are thicker than later types, as also indicated by their smaller median $\log_{10}(R_{25})$.

A dip is observed for Sbc galaxies, which seems strange since the maximum extinction is expected precisely for this type (Fioc & Rocca-Volmerange 1997). Though not

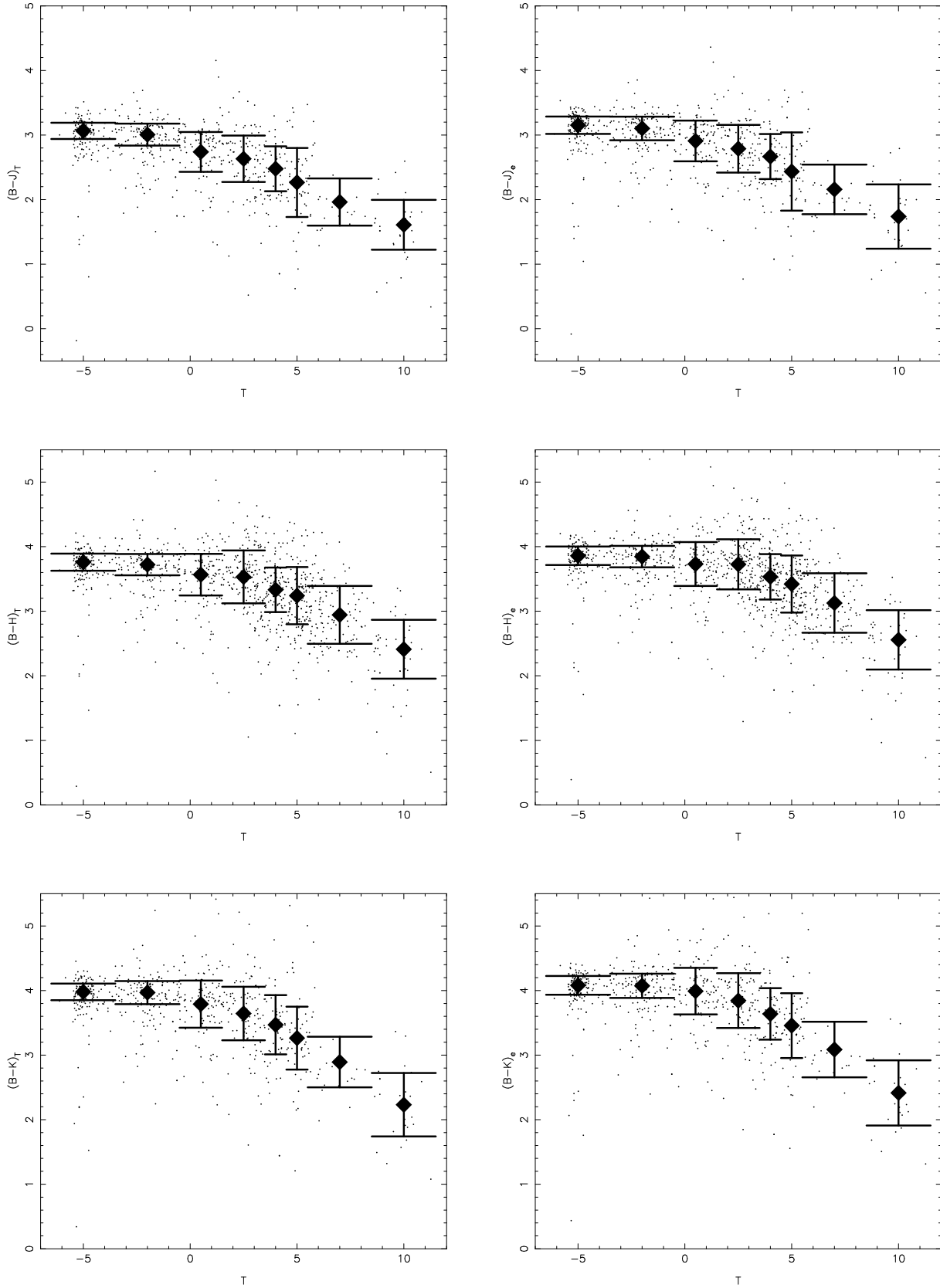


Fig. 3. Total and effective optical-to-NIR colors as a function of the type. The diamonds are the standard colors determined by ML. The vertical segments show the intrinsic scatter and the horizontal ones the width of the type-bin.

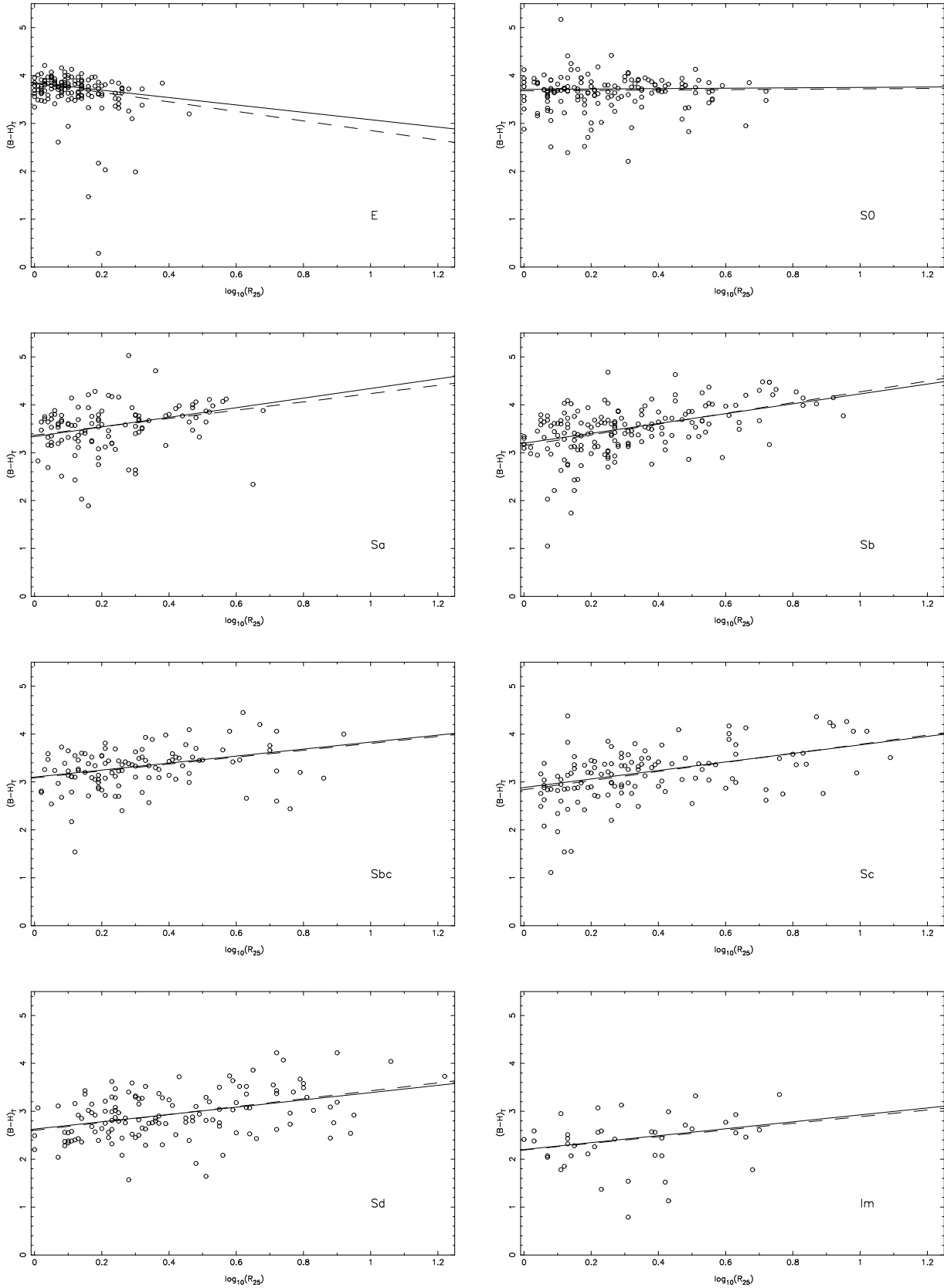


Fig. 4. $(B - H)_T$ - $\log_{10}(R_{25})$ relation per type. The solid and dashed lines correspond respectively to the ML and MCES estimators.

type	N	$\beta_0[(B - J)_T]$	σ	$\beta_0[(B - J)_e]$	σ
E	140	3.07 ± 0.02	0.13 ± 0.02	3.15 ± 0.01	0.13 ± 0.01
		<i>3.02 ± 0.02</i>	<i>0.10 ± 0.03</i>	<i>3.13 ± 0.02</i>	<i>0.14 ± 0.02</i>
S0	155	3.01 ± 0.02	0.17 ± 0.02	3.10 ± 0.02	0.18 ± 0.01
		<i>2.97 ± 0.02</i>	<i>0.15 ± 0.03</i>	<i>3.07 ± 0.02</i>	<i>0.24 ± 0.02</i>
Sa	97	2.74 ± 0.04	0.31 ± 0.03	2.91 ± 0.04	0.31 ± 0.03
		<i>2.74 ± 0.04</i>	<i>0.25 ± 0.05</i>	<i>2.93 ± 0.03</i>	<i>0.27 ± 0.03</i>
Sb	95	2.63 ± 0.04	0.36 ± 0.04	2.79 ± 0.04	0.37 ± 0.03
		<i>2.62 ± 0.05</i>	<i>0.33 ± 0.04</i>	<i>2.79 ± 0.04</i>	<i>0.36 ± 0.04</i>
Sbc	47	2.48 ± 0.06	0.35 ± 0.05	2.67 ± 0.06	0.35 ± 0.04
		<i>2.45 ± 0.06</i>	<i>0.17 ± 0.10</i>	<i>2.66 ± 0.05</i>	<i>0.26 ± 0.07</i>
Sc	46	2.27 ± 0.09	0.53 ± 0.07	2.44 ± 0.10	0.61 ± 0.07
		<i>2.24 ± 0.08</i>	<i>0.45 ± 0.10</i>	<i>2.43 ± 0.10</i>	<i>0.56 ± 0.08</i>
Sd	26	1.96 ± 0.09	0.37 ± 0.07	2.16 ± 0.09	0.38 ± 0.07
		<i>1.93 ± 0.08</i>	<i>0.23 ± 0.12</i>	<i>2.14 ± 0.08</i>	<i>0.32 ± 0.10</i>
Im	28	1.61 ± 0.09	0.39 ± 0.07	1.74 ± 0.10	0.50 ± 0.08
		<i>1.52 ± 0.10</i>	<i>0.41 ± 0.10</i>	<i>1.72 ± 0.10</i>	<i>0.47 ± 0.08</i>

Table 4. $(B - J)_T$ and $(B - J)_e$ colors per type. The values computed with the ML and MCES estimators are written respectively in boldface and italic characters. σ is the intrinsic scatter.

type	N	$\beta_0[(B - H)_T]$	σ	$\beta_0[(B - H)_e]$	σ
E	142	3.76 ± 0.02	0.13 ± 0.01	3.86 ± 0.02	0.14 ± 0.01
		<i>3.73 ± 0.02</i>	<i>0.08 ± 0.04</i>	<i>3.84 ± 0.02</i>	<i>0.13 ± 0.02</i>
S0	157	3.72 ± 0.02	0.17 ± 0.02	3.85 ± 0.02	0.17 ± 0.01
		<i>3.69 ± 0.02</i>	<i>0.14 ± 0.03</i>	<i>3.82 ± 0.02</i>	<i>0.19 ± 0.02</i>
Sa	110	3.57 ± 0.04	0.32 ± 0.03	3.73 ± 0.04	0.34 ± 0.03
		<i>3.54 ± 0.04</i>	<i>0.31 ± 0.04</i>	<i>3.73 ± 0.04</i>	<i>0.33 ± 0.03</i>
Sb	171	3.53 ± 0.03	0.41 ± 0.03	3.73 ± 0.03	0.39 ± 0.02
		<i>3.52 ± 0.03</i>	<i>0.40 ± 0.03</i>	<i>3.71 ± 0.03</i>	<i>0.40 ± 0.03</i>
Sbc	110	3.33 ± 0.04	0.34 ± 0.03	3.53 ± 0.04	0.35 ± 0.03
		<i>3.30 ± 0.03</i>	<i>0.29 ± 0.04</i>	<i>3.51 ± 0.03</i>	<i>0.32 ± 0.03</i>
Sc	125	3.24 ± 0.04	0.44 ± 0.03	3.42 ± 0.04	0.44 ± 0.03
		<i>3.20 ± 0.04</i>	<i>0.42 ± 0.04</i>	<i>3.39 ± 0.04</i>	<i>0.43 ± 0.03</i>
Sd	135	2.94 ± 0.04	0.45 ± 0.03	3.13 ± 0.04	0.46 ± 0.03
		<i>2.93 ± 0.04</i>	<i>0.45 ± 0.03</i>	<i>3.12 ± 0.04</i>	<i>0.47 ± 0.03</i>
Im	42	2.41 ± 0.08	0.46 ± 0.06	2.56 ± 0.08	0.46 ± 0.06
		<i>2.38 ± 0.08</i>	<i>0.42 ± 0.07</i>	<i>2.54 ± 0.08</i>	<i>0.44 ± 0.06</i>

Table 5. $(B - H)_T$ and $(B - H)_e$ colors per type.

inconsistent with a constant slope for all spirals, given the uncertainties, a similar dip is also obvious in the slopes of the $(B - V)_T$ - and $(U - B)_T$ - $\log_{10}(R_{25})$ relations, suggesting that this is a real phenomenon. One should first remember that the slope is not a measure of the total extinction but of the *reddening relative to face-on*. With a simple radiative transfer model where the stars and the dust are distributed homogeneously in an infinite slab, we find that when the face-on optical depth τ_V in the V -band increases, the slope begins first to steepen (Fig. 6b) but when τ_V becomes larger than 1–2, the slope flattens although the colors go on reddening (Fig. 6a). Although this modeling is simplistic and we can not infer from it the value of the optical depth, this suggests that the extinction may indeed be higher for Sbc and that the slope

has begun to decrease. This conclusion is reinforced by the fact that the slope *decreases* when we consider *effective* $B - H$ colors ($\beta_1[\log_{10}(R_{25})] = 0.60/0.55$), which are probably more extinguished than total colors.

We observe a positive slope for irregular galaxies in $B - H$, contrary to $B - V$ and $U - B$ where none is detected. However, the uncertainties are large and the null slope is within 2σ . Moreover, our “Im” type regroups in fact not only Im galaxies ($T = 10$) but also Sm ($T = 9$) which are more elongated and redder. The small size of the “Im” sample makes it impossible to decide whether this reddening is due to the dust or to intrinsically redder populations in Sm galaxies.

No slope is observed for lenticular galaxies, which may indicate that no significant amount of dust is present in S0

type	N	$\beta_0[(B - K)_T]$	σ	$\beta_0[(B - K)_e]$	σ
E	142	3.98 ± 0.02	0.13 ± 0.01	4.08 ± 0.02	0.15 ± 0.01
		3.95 ± 0.02	0.09 ± 0.04	4.06 ± 0.02	0.14 ± 0.02
S0	159	3.97 ± 0.02	0.18 ± 0.02	4.07 ± 0.02	0.19 ± 0.01
		3.95 ± 0.02	0.15 ± 0.03	4.06 ± 0.02	0.19 ± 0.02
Sa	99	3.79 ± 0.04	0.37 ± 0.03	3.99 ± 0.04	0.36 ± 0.03
		3.79 ± 0.04	0.33 ± 0.04	4.00 ± 0.04	0.35 ± 0.03
Sb	100	3.64 ± 0.05	0.41 ± 0.04	3.84 ± 0.05	0.42 ± 0.04
		3.62 ± 0.05	0.42 ± 0.05	3.82 ± 0.05	0.43 ± 0.04
Sbc	48	3.47 ± 0.08	0.46 ± 0.06	3.64 ± 0.07	0.40 ± 0.05
		3.45 ± 0.07	0.32 ± 0.10	3.64 ± 0.06	0.32 ± 0.06
Sc	46	3.26 ± 0.09	0.49 ± 0.07	3.46 ± 0.09	0.50 ± 0.06
		3.22 ± 0.08	0.39 ± 0.10	3.43 ± 0.08	0.45 ± 0.07
Sd	24	2.89 ± 0.10	0.39 ± 0.08	3.09 ± 0.10	0.43 ± 0.08
		2.80 ± 0.08	0.21 ± 0.13	3.01 ± 0.09	0.31 ± 0.10
Im	25	2.23 ± 0.11	0.49 ± 0.09	2.41 ± 0.11	0.50 ± 0.08
		2.21 ± 0.11	0.45 ± 0.10	2.40 ± 0.11	0.50 ± 0.08

Table 6. $(B - K)_T$ and $(B - K)_e$ colors per type.

type	N	$\beta_0[(B - H)_T]$	$\beta_1[\log_{10}(R_{25})]$	μ_1	σ
E	138	3.77 ± 0.02	-0.77 ± 0.19	0.10	0.12 ± 0.01
		3.75 ± 0.02	-1.00 ± 0.27		(0.03 ± 0.03)
S0	153	3.72 ± 0.02	0.04 ± 0.11	0.20	0.17 ± 0.02
		3.69 ± 0.02	0.04 ± 0.12		0.15 ± 0.03
Sa	110	3.53 ± 0.04	1.00 ± 0.22	0.19	0.31 ± 0.03
		3.53 ± 0.04	0.87 ± 0.19		0.24 ± 0.04
Sb	171	3.48 ± 0.03	1.03 ± 0.14	0.27	0.34 ± 0.02
		3.45 ± 0.03	1.12 ± 0.14		0.34 ± 0.03
Sbc	110	3.29 ± 0.04	0.73 ± 0.19	0.25	0.34 ± 0.03
		3.27 ± 0.03	0.72 ± 0.22		0.28 ± 0.04
Sc	125	3.14 ± 0.04	0.89 ± 0.15	0.29	0.37 ± 0.03
		3.12 ± 0.04	0.95 ± 0.17		0.32 ± 0.03
Sd	135	2.89 ± 0.04	0.76 ± 0.15	0.34	0.40 ± 0.03
		2.88 ± 0.04	0.82 ± 0.16		0.38 ± 0.03
Im	41	2.41 ± 0.08	0.72 ± 0.36	0.29	0.40 ± 0.06
		2.39 ± 0.07	0.70 ± 0.34		0.35 ± 0.08

Table 7. $(B - H)_T$ color per type as a function of $X_{i1} = \log_{10}(R_{25})$.

(see also Sandage & Visvanathan 1978). Another possibility is that the disk is overwhelmed by the bulge. No inclination dependence of the colors would then be expected if the bulge is spherically symmetric or if it is devoid of dust.

The most striking result is the negative slope observed for ellipticals. This certainly does not come from the dust because the slope would be positive. For ellipticals, R_{25} is not directly related to the inclination because their true shape is unknown. In the mean, rounder ellipticals seem redder and are probably more metal-rich (Terlevich et al. 1980). They also tend to be brighter (Tremblay & Merritt 1996) which may link the color- $\log_{10}(R_{25})$ relation of ellipticals to their color-magnitude relation. No such relation is observed in $B - V$, which is anyway a poor indicator of the metallicity. The $(U - B)_T$ - $\log_{10}(R_{25})$ is not very conclusive: whereas the ML estimator provides a negative

slope, as in $B - H$, the MCES estimator does not detect any. Since no obvious bias between the two estimators is observed for the other types and the intrinsic scatter is very small compared to the uncertainties on the colors for ellipticals – which is the worst case for the MCES estimators –, we tend to trust more the result given by the ML.

5.5. The color-magnitude relation

5.5.1. Global relation

The color-magnitude (CM) relation is an important constraint on the dynamical models of galaxy formation for the absolute magnitude may be related to the mass of the galaxy via a mass-to-luminosity ratio. An important question is the choice of the reference band, optical or

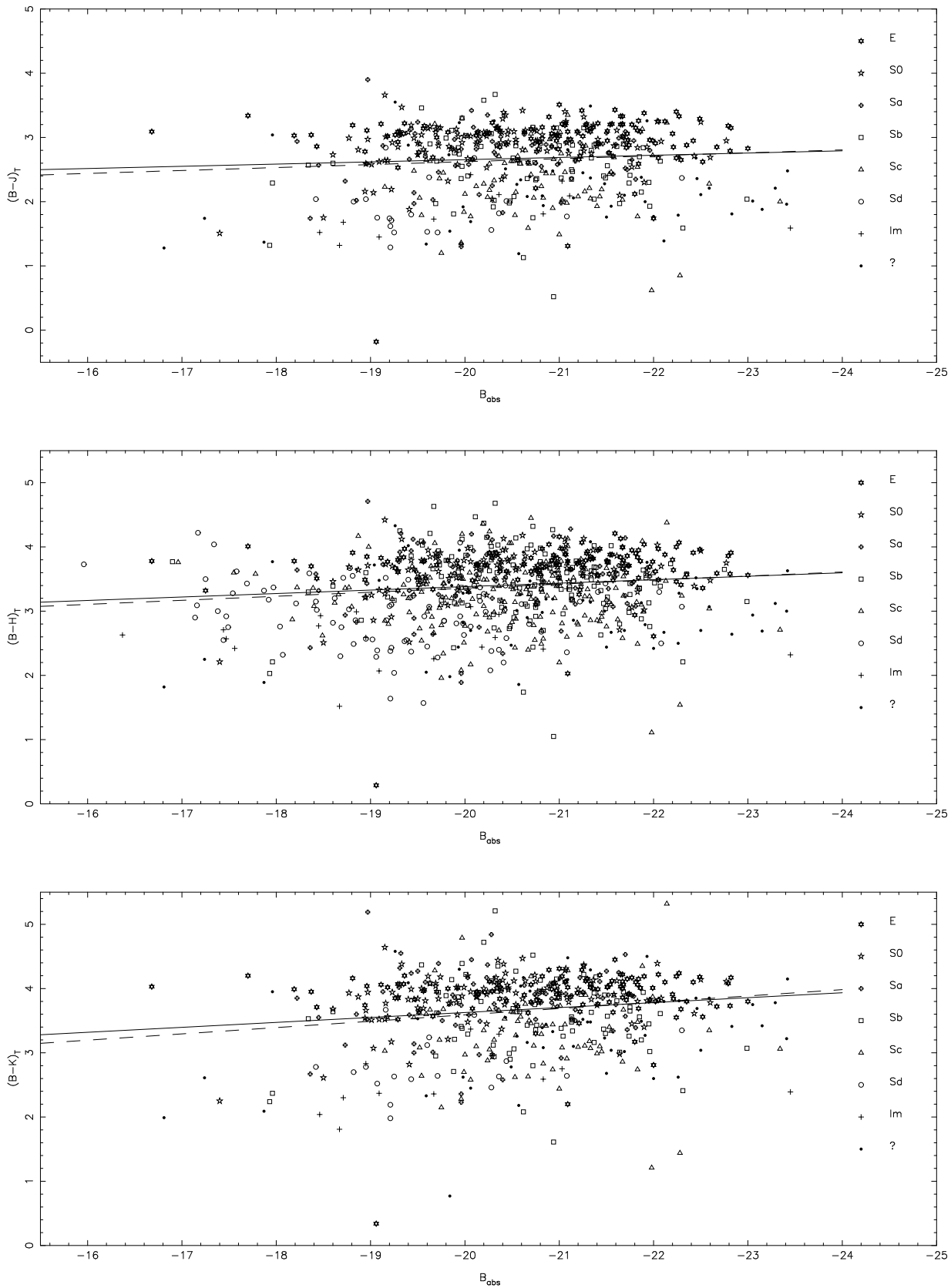


Fig. 7. Global $(B - \text{NIR})_T$ -absolute B magnitude relations.

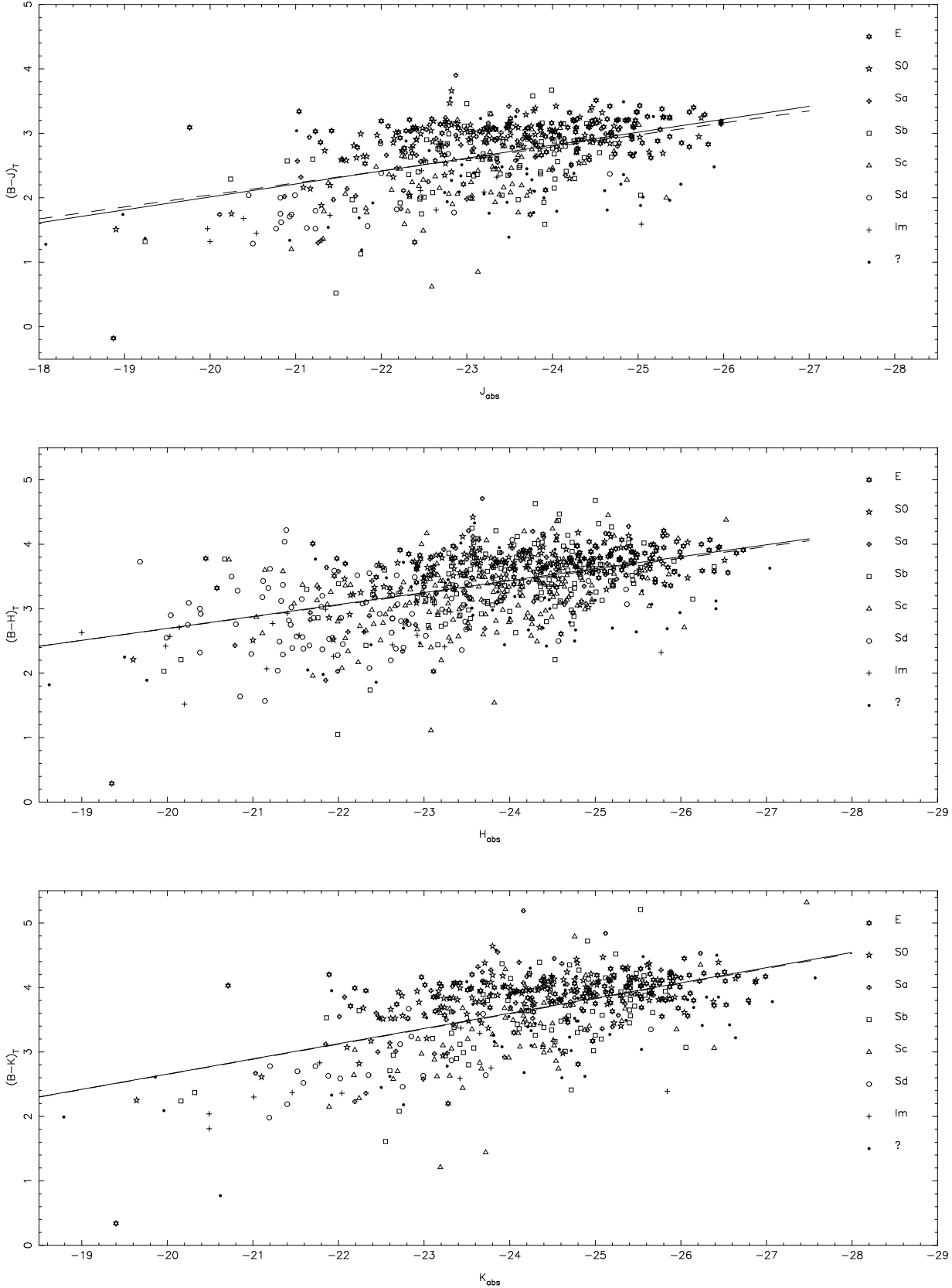


Fig. 8. Global $(B - \text{NIR})_T$ -absolute NIR magnitude relations.

$(B - \text{NIR})_T$	N	$\beta_0[(B - \text{NIR})_T]$	$\beta_1(B_{\text{abs}})$	μ_1	σ	$\beta_0[(B - \text{NIR})_T]$	$\beta_1(\text{NIR}_{\text{abs}})$	μ_1	σ
$(B - J)_T$	540	2.68 ± 0.02	-0.03 ± 0.02	-20.67	0.47 ± 0.02	2.68 ± 0.02	-0.20 ± 0.02	-23.34	0.41 ± 0.01
		$2.65 ± 0.02$	$-0.05 ± 0.03$		$0.46 ± 0.02$	$2.67 ± 0.02$	$-0.19 ± 0.02$		$0.40 ± 0.02$
$(B - H)_T$	814	3.41 ± 0.02	-0.05 ± 0.01	-20.46	0.45 ± 0.01	3.42 ± 0.02	-0.19 ± 0.01	-23.90	0.40 ± 0.01
		$3.39 ± 0.02$	$-0.06 ± 0.02$		$0.45 ± 0.01$	$3.40 ± 0.01$	$-0.18 ± 0.01$		$0.40 ± 0.01$
$(B - K)_T$	546	3.68 ± 0.02	-0.08 ± 0.02	-20.67	0.49 ± 0.02	3.69 ± 0.02	-0.24 ± 0.01	-24.38	0.41 ± 0.01
		$3.66 ± 0.02$	$-0.10 ± 0.03$		$0.49 ± 0.02$	$3.68 ± 0.02$	$-0.23 ± 0.02$		$0.40 ± 0.01$

Table 8. $(B - \text{NIR})_T$ vs. B_{abs} or NIR_{abs} color-magnitude relations, where $\text{NIR} = J, H$ or K .

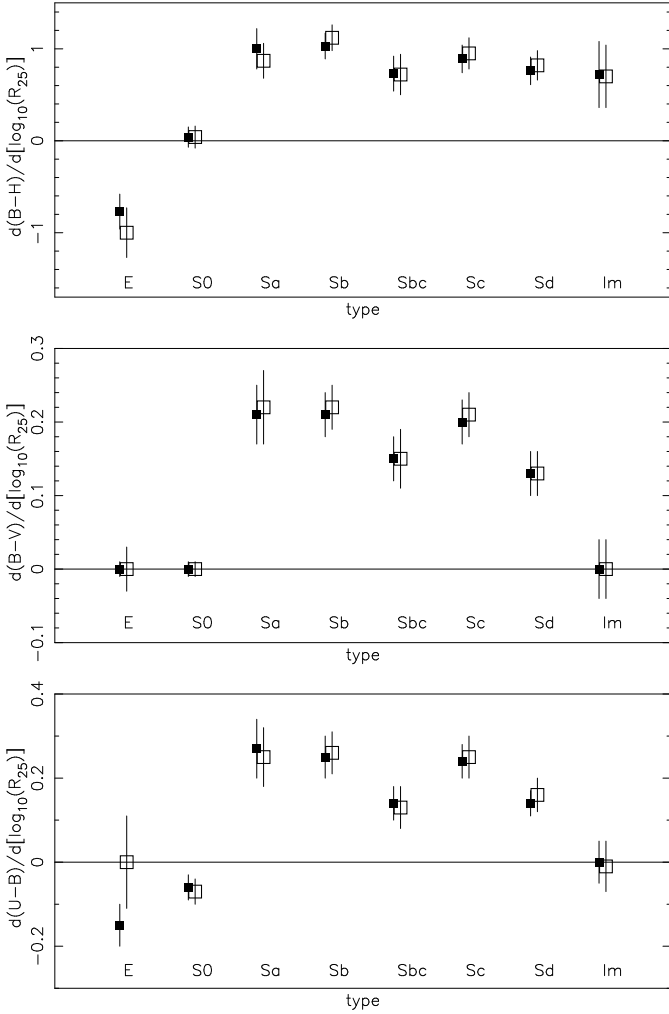


Fig. 5. Slopes of the $(B - H)_T$ -, $(B - V)_T$ -, and $(U - B)_T$ - $\log_{10}(R_{25})$ relations as a function of type. The black and white squares correspond respectively to the ML and MCES estimators.

NIR, used for the absolute magnitude. Usually, the NIR has been adopted because it suffers little extinction. Another reason is that it is produced mainly by old giants and is therefore expected to be a better indicator of the mass than the optical, which is more sensitive to the recent star formation. We have plotted on Figs. 7 and 8 the color-absolute magnitude relation with either the optical

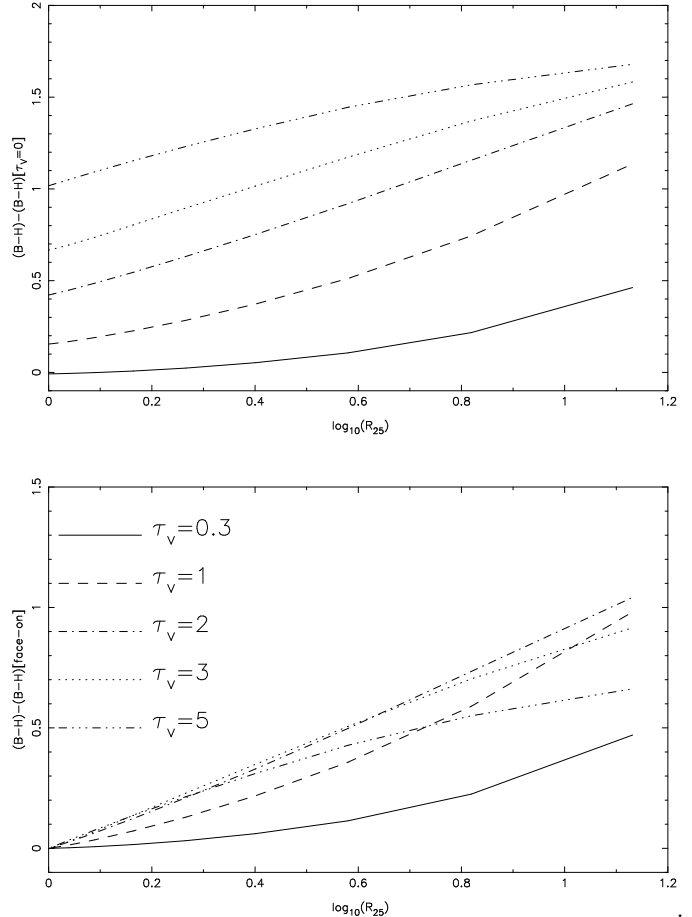


Fig. 6. $(B - H)$ - $\log_{10}(R_{25})$ relations computed with the radiative transfer code (see text) for different face-on V -band optical depths. We assume $q_0 = 0.18$, a typical value for an Sb. **Top:** reddening relative to the dust-free case. **Bottom:** reddening relative to face-on.

or the NIR as reference band. The corresponding estimators are given in Table 8. The $(B - \text{NIR})_T$ - NIR_{abs} relation is much steeper than the $(B - \text{NIR})_T$ - B_{abs} one. If there was no intrinsic scatter, the slopes should be nearly the same. For example, if $(B - \text{NIR})_T = \alpha \text{NIR}_{\text{abs}} + \kappa$, then we should have $(B - \text{NIR})_T = [\alpha/(1 + \alpha)](B_{\text{abs}} + \kappa)$, which has almost the same slope since $|\alpha| \ll 1$. The scatter is moreover smaller when the NIR is the reference band. To detect a color-magnitude relation, the choice of the NIR as

reference band is thus clearly favored. Though the overall agreement is very good, we note that the ML estimator of the slope is slightly biased when compared to the *a priori* unbiased MCES estimator. Its slope is “more positive” in the $(B - \text{NIR})_{\text{T}} - B_{\text{abs}}$ relation because of the positive correlation of the errors in $(B - \text{NIR})_{\text{T}}$ and B_{abs} , and “more negative” in the $(B - \text{NIR})_{\text{T}} - \text{NIR}_{\text{abs}}$ relation because of the negative correlation of the errors in $(B - \text{NIR})_{\text{T}}$ and NIR_{abs} .

The slope of the $(B - \text{NIR})_{\text{T}}$ -absolute magnitude relation increases with the wavelength of the NIR band for there is also a CM relation in the NIR colors. This effect is less apparent in $(B - H)_{\text{T}}$ because the $B - H$ sample contains many late-type galaxies which have a flatter slope: a linear fit for all the galaxies together is hence too simplistic.

5.5.2. Relation per type

The global color-magnitude relation discussed above is actually dominated by star-forming galaxies ($\beta_1(H_{\text{abs}}) = -0.21/-0.20$ against $-0.07/-0.05$ for E/S0). These values are close to the slopes of the $(B_{\text{j}} - K)[D_{25}] - K_{\text{abs}}$ relations (-0.24 ± 0.03 for Sa–Sdm and -0.09 ± 0.04 for E/S0) determined by Mobasher et al. (1986). The slope for spiral galaxies is much steeper than the relations obtained by Bershady (1995) for its spectral types bk, bm, am and fm. This is however not surprising, because using *spectral* types rather than *photometric* types bins galaxies as a function of their colors and tends to suppress any color-magnitude relation.

An especially interesting question is whether the mass is the main driving force of galaxy evolution and star formation, or if the galaxy type has also to be considered. To answer this question, it is worth to look at the color-magnitude relation per type more thoroughly. We have plotted the $(B - H)_{\text{T}} - H_{\text{abs}}$ relation as a function of type in Fig. 9. We also show in Fig. 10 the $(B - H)_{\text{T}}^0 - H_{\text{abs}}$ relations where $(B - H)_{\text{T}}^0$ is the color corrected to face-on using the $\beta_1[\log_{10}(R_{25})]$ determined in 5.4. We assume that the extinction is negligible in the NIR and do not correct H_{abs} . No correction is also applied to elliptical colors because their color- R_{25} relation is not due to the extinction. The values of the estimators are given in Table 9. We note that the intrinsic scatter in the corrected colors is significantly reduced. A more picturesque comparison of the relations for the different types is plotted on Fig. 11. Though the agreement between the estimators is not as good as previously and the uncertainties are large, the slope obviously depends on the type. We tentatively summarize the following results:

Star-forming galaxies: the slope is much flatter for Sd–Im than for Sa–Sc galaxies. Mobasher et al. (1986) probably did not detect this because the few Sd/Im galaxies in their

late-spirals sample were lost among Sbc and Sc galaxies. At a given NIR absolute magnitude, the mean colors of the types are different, indicating that the CM relation is not simply a type-mass relation: the NIR intrinsic luminosity must be completed by the type to characterize the colors (and the star formation history) of star-forming galaxies. A similar conclusion was drawn by Gavazzi (1993) but was later challenged by Gavazzi et al. (1996b).

E/S0: the color-magnitude relation of early-type galaxies is usually explained by the galactic winds produced by super-novae in a starbursting environment, which expel the gas and quench the star formation (Matthews & Baker 1971). Massive (and NIR bright) galaxies having a deeper gravitational well, they are able to retain the gas longer and to prolong the star-forming phase. This results in a higher mean stellar metallicity and thus in redder colors (Faber 1973). Besides its interest to constrain the models of galaxy formation, the CM relation has also been proposed as a distance indicator.

We find a different slope for ellipticals and lenticulars. The slope of S0 seems closer to that of early and intermediate spirals than to that of ellipticals, which may give some clues on their evolution.

The MCES estimation does not detect any significant slope for ellipticals. Because of the small intrinsic scatter, it is maybe not the best estimator², but even the slope determined by ML is smaller than that of the comparable $(V - K)[5h^{-1} \text{ kpc}] - V_{\text{T}}$ relation established by Bower et al. (1992) in the Virgo and Coma clusters. Our intrinsic scatter is also larger than theirs. A possible explanation of this discrepancy is that our sample contains not only cluster galaxies but also field ellipticals, which may have a different star formation history and increase the scatter (Larson et al. 1980; Kauffmann & Charlot 1998; Baugh et al. 1996; see yet Bernardi et al. 1998 and Schade et al. 1996). However, we also note that the relation established by Bower et al. is based on *aperture* colors. Their aperture is comparable to the mean effective aperture of ellipticals in Virgo and samples only about half their luminosity (cf. also Kodama et al. 1997). Since the effective aperture of bright ellipticals is larger, only their inner regions are observed in the Bower et al.’s aperture. Because of the blue-outwards color gradient, their aperture color is redder and the slope is higher than the one derived from total colors. We therefore encourage the modellists of elliptical galaxies, either to compare their relations to total observed colors, or to predict aperture colors.

The color-magnitude relations as a function of the B absolute magnitude are finally plotted for each type on

² Note that the slopes obtained for the *effective* color vs. absolute magnitude relation with the two estimators ($-0.03/-0.02$) are in good agreement, both between them and with the MCES slope of the total color-magnitude relation.

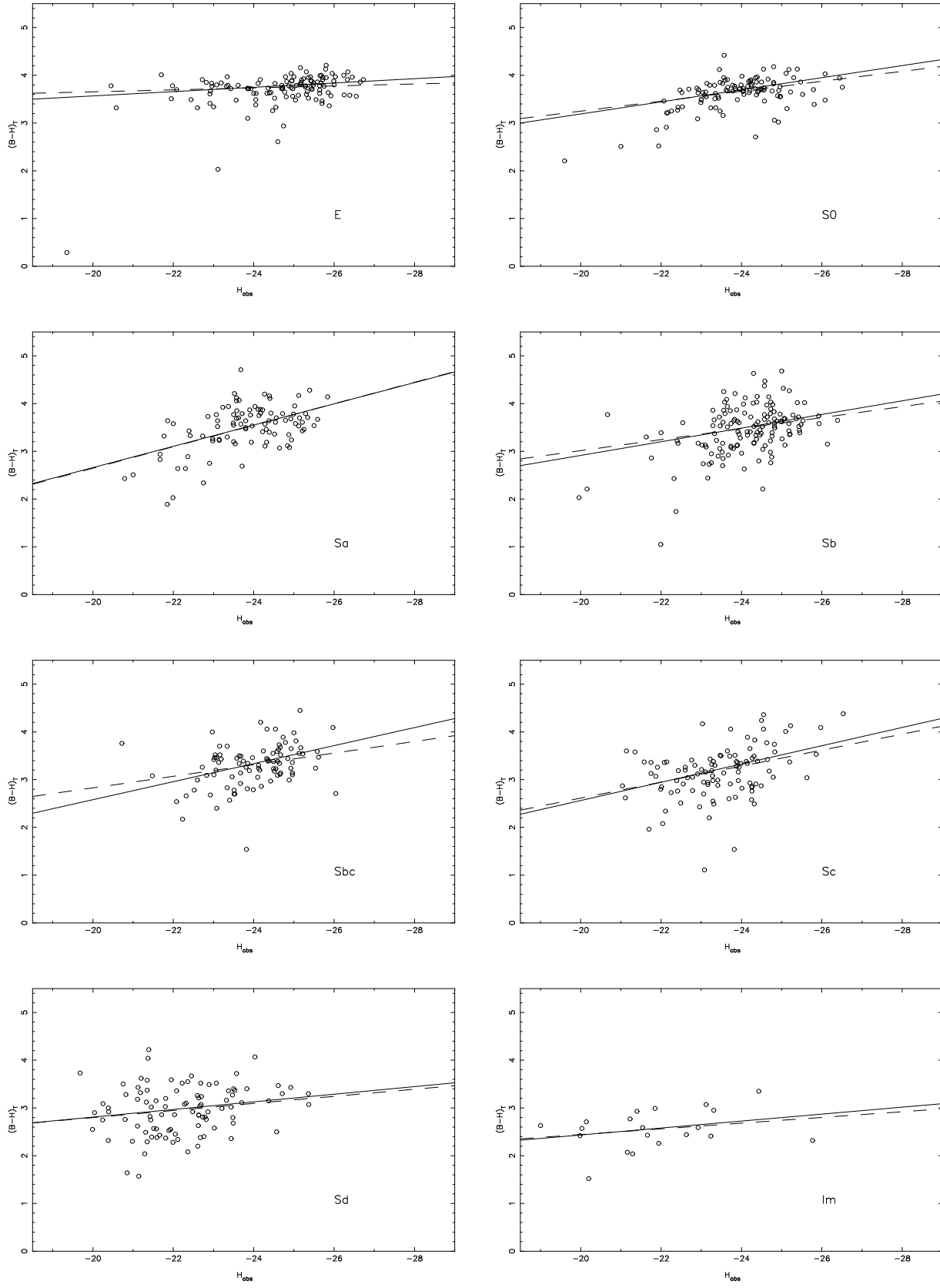


Fig. 9. $(B - H)_T$ -absolute H magnitude relations per type.

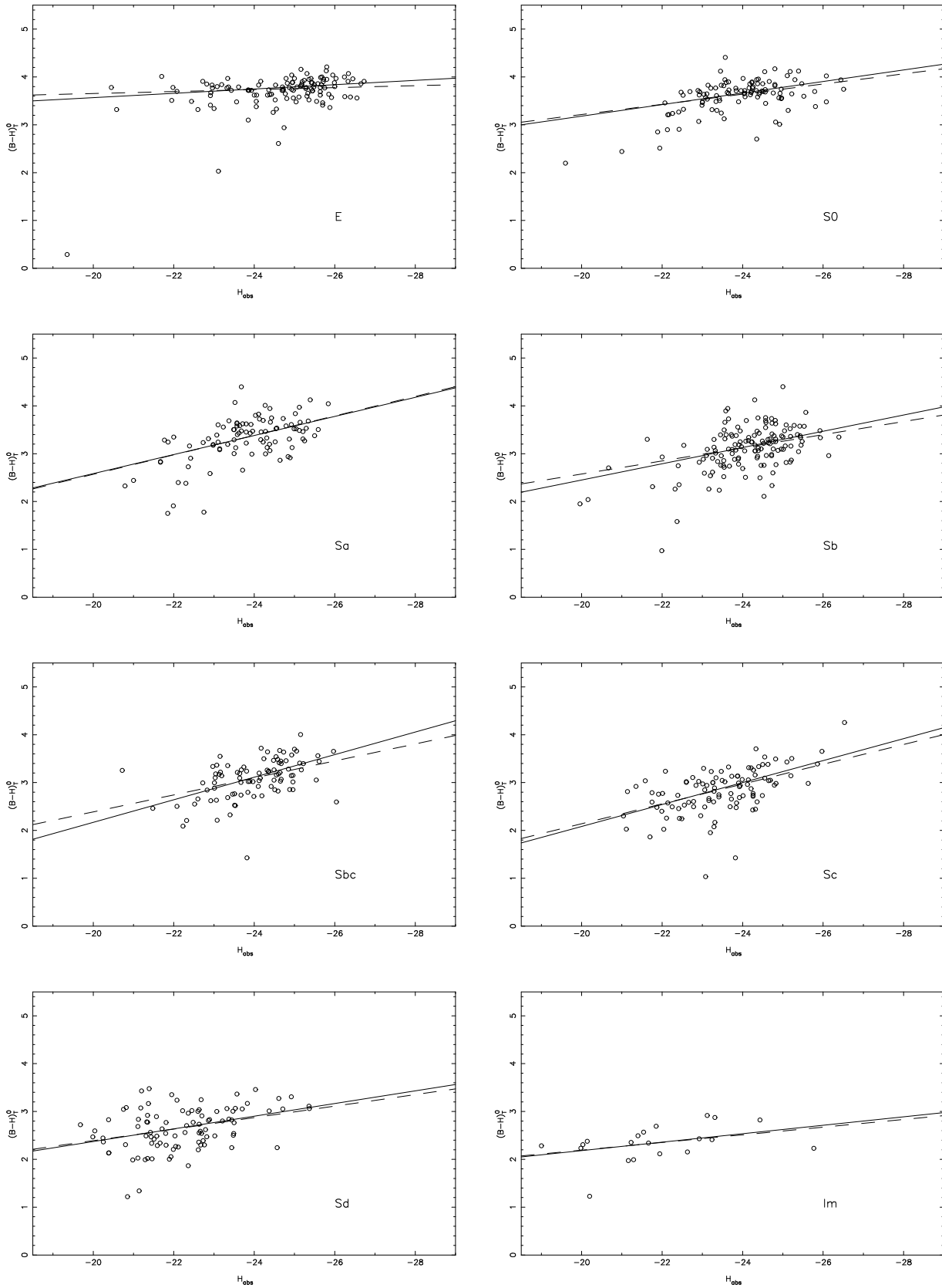


Fig. 10. $(B - H)_T^0$ -absolute H magnitude relations per type.

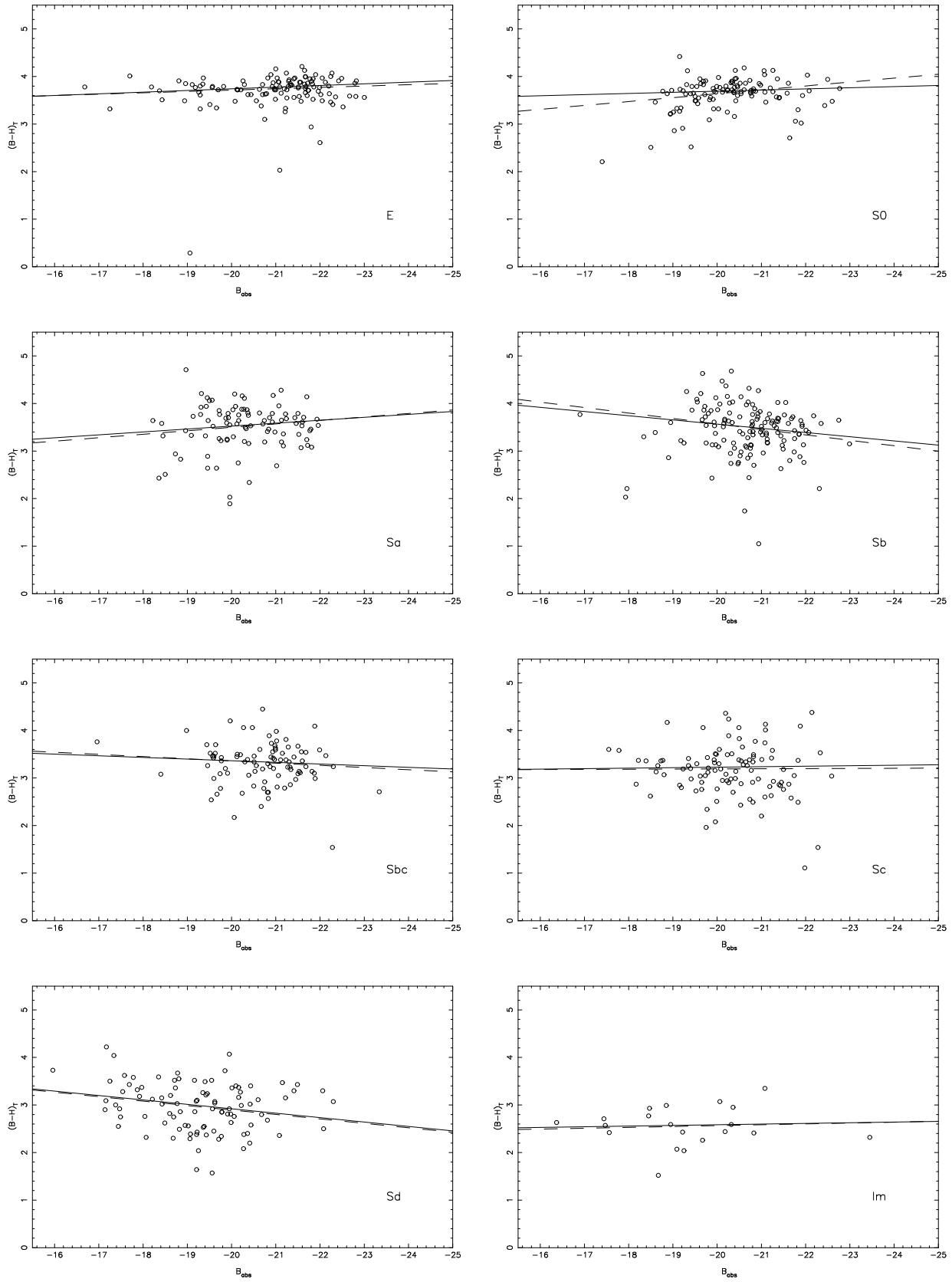


Fig. 12. $(B - H)_T$ -absolute B magnitude relations per type.

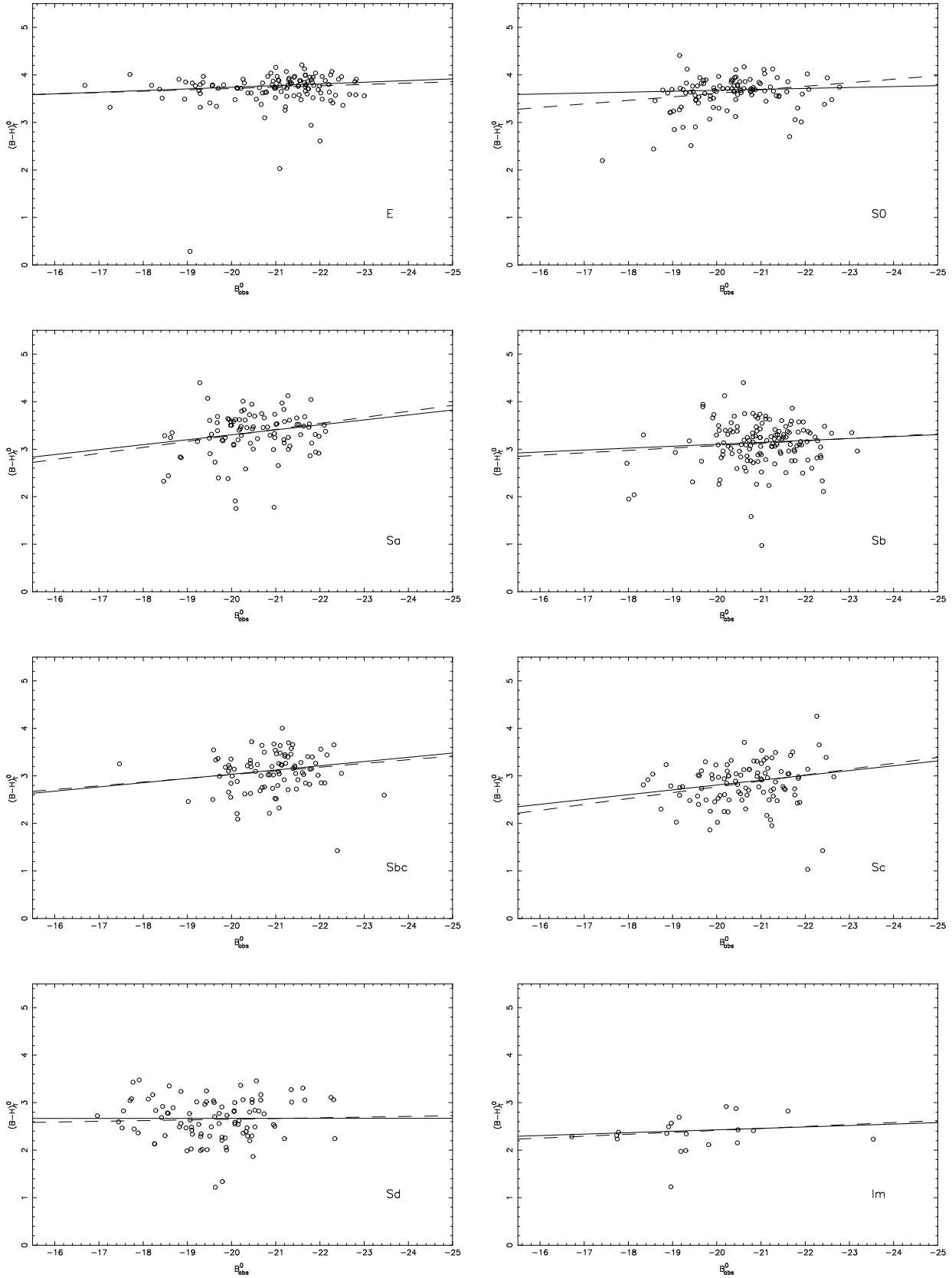


Fig. 13. $(B-H)_T^0$ -absolute B^0 magnitude relations per type.

type	N	$\beta_0[(B - H)_T]$	$\beta_1(H_{\text{abs}})$	μ_1	σ	$\beta_0[(B - H)_T^0]$	$\beta_1(H_{\text{abs}})$	σ
E	119	3.79 ± 0.02	-0.05 ± 0.01	-24.95	0.12 ± 0.02	3.79 ± 0.02	-0.05 ± 0.01	0.12 ± 0.02
		<i>3.76 ± 0.02</i>	<i>-0.02 ± 0.02</i>		<i>(0.06 ± 0.04)</i>	<i>3.76 ± 0.02</i>	<i>-0.02 ± 0.02</i>	<i>(0.06 ± 0.04)</i>
S0	110	3.70 ± 0.02	-0.13 ± 0.02	-24.00	0.14 ± 0.02	3.67 ± 0.02	-0.12 ± 0.02	0.18 ± 0.02
		<i>3.67 ± 0.02</i>	<i>-0.10 ± 0.03</i>		<i>0.14 ± 0.03</i>	<i>3.64 ± 0.02</i>	<i>-0.11 ± 0.03</i>	<i>0.16 ± 0.03</i>
Sa	94	3.52 ± 0.04	-0.22 ± 0.04	-23.85	0.37 ± 0.03	3.35 ± 0.04	-0.20 ± 0.03	0.29 ± 0.03
		<i>3.51 ± 0.04</i>	<i>-0.22 ± 0.05</i>		<i>0.36 ± 0.04</i>	<i>3.35 ± 0.04</i>	<i>-0.20 ± 0.05</i>	<i>0.28 ± 0.04</i>
Sb	140	3.53 ± 0.04	-0.14 ± 0.04	-24.31	0.37 ± 0.03	3.18 ± 0.03	-0.17 ± 0.03	0.30 ± 0.02
		<i>3.51 ± 0.04</i>	<i>-0.12 ± 0.05</i>		<i>0.36 ± 0.03</i>	<i>3.17 ± 0.03</i>	<i>-0.14 ± 0.04</i>	<i>0.29 ± 0.03</i>
Sbc	91	3.36 ± 0.04	-0.19 ± 0.04	-24.12	0.35 ± 0.03	3.14 ± 0.03	-0.24 ± 0.03	0.26 ± 0.03
		<i>3.33 ± 0.04</i>	<i>-0.12 ± 0.07</i>		<i>0.32 ± 0.04</i>	<i>3.12 ± 0.03</i>	<i>-0.18 ± 0.06</i>	<i>0.25 ± 0.03</i>
Sc	102	3.22 ± 0.04	-0.19 ± 0.04	-23.44	0.39 ± 0.03	2.87 ± 0.03	-0.23 ± 0.03	0.27 ± 0.03
		<i>3.19 ± 0.04</i>	<i>-0.17 ± 0.05</i>		<i>0.38 ± 0.03</i>	<i>2.85 ± 0.03</i>	<i>-0.21 ± 0.04</i>	<i>0.25 ± 0.03</i>
Sd	95	2.98 ± 0.05	-0.08 ± 0.04	-22.11	0.46 ± 0.04	2.65 ± 0.04	-0.13 ± 0.03	0.37 ± 0.03
		<i>2.95 ± 0.05</i>	<i>-0.07 ± 0.05</i>		<i>0.46 ± 0.04</i>	<i>2.64 ± 0.04</i>	<i>-0.12 ± 0.04</i>	<i>0.34 ± 0.03</i>
Im	20	2.55 ± 0.09	-0.07 ± 0.05	-21.60	0.34 ± 0.07	2.32 ± 0.08	-0.09 ± 0.04	0.27 ± 0.06
		<i>2.54 ± 0.08</i>	<i>-0.06 ± 0.07</i>		<i>0.31 ± 0.09</i>	<i>2.32 ± 0.08</i>	<i>-0.08 ± 0.06</i>	<i>0.24 ± 0.11</i>

Table 9. $(B - H)_T$ and $(B - H)_T^0$ per type as a function of $X_{i1} = H_{\text{abs}}$.

type	N	$\beta_0[(B - H)_T]$	$\beta_1(H_{\text{abs}})$	μ_1	$\beta_2[\log_{10}(R_{25})]$	μ_2	σ
E	115	3.80 ± 0.02	-0.05 ± 0.01	-24.97	-0.67 ± 0.19	0.10	0.10 ± 0.02
		<i>3.76 ± 0.02</i>	<i>-0.02 ± 0.02</i>		<i>-0.83 ± 0.35</i>		<i>(0.04 ± 0.03)</i>
S0	106	3.66 ± 0.02	-0.16 ± 0.02	-24.05	0.37 ± 0.16	0.19	0.18 ± 0.02
		<i>3.66 ± 0.02</i>	<i>-0.12 ± 0.04</i>		<i>0.27 ± 0.17</i>		<i>0.14 ± 0.03</i>
Sa	94	3.47 ± 0.04	-0.23 ± 0.03	-23.85	1.18 ± 0.23	0.17	0.30 ± 0.03
		<i>3.49 ± 0.04</i>	<i>-0.21 ± 0.04</i>		<i>1.21 ± 0.20</i>		<i>0.27 ± 0.04</i>
Sb	140	3.47 ± 0.03	-0.17 ± 0.03	-24.31	0.97 ± 0.13	0.25	0.30 ± 0.02
		<i>3.45 ± 0.03</i>	<i>-0.14 ± 0.04</i>		<i>0.99 ± 0.13</i>		<i>0.29 ± 0.02</i>
Sbc	91	3.30 ± 0.03	-0.28 ± 0.03	-24.12	1.22 ± 0.16	0.25	0.23 ± 0.03
		<i>3.28 ± 0.03</i>	<i>-0.22 ± 0.06</i>		<i>1.19 ± 0.21</i>		<i>0.24 ± 0.03</i>
Sc	102	3.13 ± 0.04	-0.24 ± 0.03	-23.44	1.10 ± 0.13	0.29	0.27 ± 0.03
		<i>3.11 ± 0.03</i>	<i>-0.22 ± 0.04</i>		<i>1.17 ± 0.14</i>		<i>0.24 ± 0.03</i>
Sd	95	2.91 ± 0.04	-0.14 ± 0.03	-22.11	1.15 ± 0.16	0.32	0.33 ± 0.03
		<i>2.88 ± 0.04</i>	<i>-0.15 ± 0.04</i>		<i>1.23 ± 0.16</i>		<i>0.33 ± 0.03</i>
Im	20	2.52 ± 0.07	-0.07 ± 0.04	-21.60	1.11 ± 0.29	0.25	0.18 ± 0.05
		<i>2.53 ± 0.06</i>	<i>-0.05 ± 0.05</i>		<i>1.09 ± 0.29</i>		<i>(0.04 ± 0.06)</i>

Table 10. $(B - H)_T$ color per type as a function of $X_{i1} = H_{\text{abs}}$ and $X_{i2} = \log_{10}(R_{25})$.

figure 12. The slopes are very different of those obtained when the NIR is the reference band. For spiral galaxies especially, they tend to have a positive sign, with brighter galaxies (in B) being bluer! This behavior is typically expected if the relation is dominated by the extinction. If we assume that the extinction is negligible in the NIR, the same correction applied to colors may be used to compute face-on absolute magnitudes B_{abs}^0 . The $(B - H)_T^0$ - B_{abs}^0 relations per type show then more reasonable slopes (Fig. 13).

5.6. The color vs. R_{25} & absolute magnitude relation

We finally give in Table 10 the estimators for a simultaneous fitting of the $(B - H)_T$ colors as a function of $\log_{10}(R_{25})$ and H_{abs} in each type. The overall agreement

with the slopes determined previously from the separate fitting of the colors with respect to either R_{25} or H_{abs} is correct. The requirement that H_{abs} be known tends to select the brightest galaxies and may explain the small discrepancies in the slope as a function of $\log_{10}(R_{25})$, as this one depends probably also on the mass ($\sim H_{\text{abs}}$) of the galaxy. The very small scatter obtained for Im galaxies indicates that there are too few of them for the simultaneous analysis.

6. Discussion

NIR growth curves of the magnitude as a function of the aperture have been built from the Catalog of Infrared Observations (Gezari et al. 1997) and optical catalogs. Using these, we have been able to compute total NIR apparent and absolute magnitudes, NIR and optical-to-NIR colors,

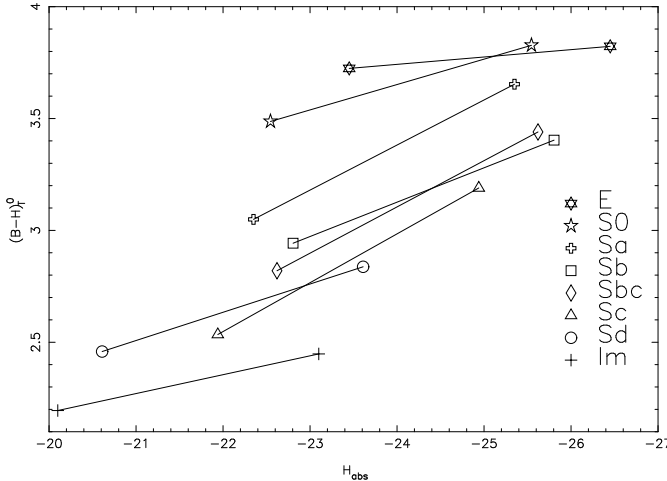


Fig. 11. Analytical $(B - H)_T^0$ -absolute H magnitude relations. The segments correspond to the mean of the ML and MCES fits and extend from $\mu_0(H_{\text{abs}}) + 1.5$ to $\mu_0(H_{\text{abs}}) - 1.5$ for each type.

and to estimate their uncertainties for a large sample. A statistical analysis of the colors as a function of type, inclination and luminosity, using estimators taking into account the uncertainties in the variables and the intrinsic scatter in the colors, highlights the interest of the NIR and notably of the comparison of the optical to the NIR.

Optical-to-NIR colors show a well defined sequence with type: the mean irregular is 1.3 magnitude bluer in $B - H$ than the mean elliptical. The intrinsic scatter is higher for star-forming galaxies ($\sigma \sim 0.4$) than for ellipticals or lenticulars ($\sigma \sim 0.1$ –0.2).

Because of the small extinction in the NIR, the optical-to-NIR colors of spiral galaxies redden considerably with increasing inclination, putting therefore constraints on the amount of the dust and the respective distributions of dust and stars. S0 colors do not depend on the inclination. Rounder elliptical are redder than more elongated ones.

The color-absolute magnitude relation is much steeper and tighter when the NIR is used as the reference band rather than the optical. Examination of the color vs. B absolute magnitude relation for each type suggests that this is due to the extinction which dims and reddens the galaxies and counteracts the color-NIR relation. A color-magnitude relation exists in each type, with brighter galaxies in the NIR being redder. The slope is steeper for Sa–Sc than for early-type galaxies or Sd–Im. The relation we obtain for ellipticals is shallower than in other studies. A likely explanation is that this is due to the effect of the color gradient in small apertures, a lesser, i.e. redder, fraction of the galaxy being observed in large bright ellipticals than in small faint ones – a problem we do not have using our total (or we expect so) colors. The slope for S0 galaxies is closer to that of spirals than to that of ellipticals. The color at a given absolute magnitude be-

comes bluer with increasing type, indicating that both the mass and the type must be used to characterize the colors and to describe the star formation history of galaxies. Once corrected for the inclination and the magnitude effect, the intrinsic scatter in the colors of spiral types drops significantly, although a few outliers with very blue colors typical of starbursting galaxies remain.

However satisfying these results are, some problems still exist. NIR observations are obtained in small apertures and the extrapolation to total magnitudes and colors suffers from significant uncertainties. Nevertheless, we do not believe that our results strongly depend on this extrapolation since similar slopes are obtained when we use effective colors – which are interpolated or only slightly extrapolated – instead of total colors.

The selection of galaxies is a more crucial problem. The only criterion used here has been to take whatever was available in the NIR. For this reason, the sample, especially in J and K , contains few late-type galaxies but many cluster galaxies, Seyferts and other active nuclei. We also lack of intrinsically faint galaxies. The color-magnitude relations we have determined should therefore not be extrapolated at H_{abs} fainter than ~ -20 . Large samples as the Sloan Digital Sky Survey in the optical or DENIS and 2MASS in the NIR should solve this problem.

The last important problem is the bias between the two estimators we use, especially in the slope of the color-magnitude relation. The discrepancy tends to disappear however when we consider effective colors which have smaller uncertainties. The MCES estimators seem to be closer to the true slopes than the ML, but the latter provides a better estimate of the intrinsic scatter and has a lower variance.

Combining the NIR and the optical enlarges considerably our vision of the stellar populations and the dust content of galaxies. In our next paper, we will extend our analysis to the near ultraviolet-optical wavelength range. We will publish “color” energy distributions of galaxies from the near-UV to the NIR that will be used as templates to constrain the star formation history of galaxies of different types and masses. A further step will be the extension of these techniques to the far-UV and the far-IR.

Acknowledgements. This research has made use of:

- the Catalog of Infrared Observations operated at the NASA/Goddard Space Flight Center (Gezari et al. 1997),
- the Hypercat catalog operated at the CRAL-Observatoire de Lyon (Prugniel & Héraudeau 1998),
- the Third Reference Catalog of Bright Galaxies (de Vaucouleurs G. et al. 1991),
- the NASA/IPAC Extragalactic Database (NED) which is operated by the Jet Propulsion Laboratory, California Institute of Technology, under contract with the National Aeronautics and Space Administration.

We also acknowledge:

- the Statistical Consulting Center for Astronomy operated at the Department of Statistics, Penn State University, M.G. Akritas (Director),
- Numerical Recipes by Press et al. (1992).

M. F. acknowledges support from the National Research Council through the Resident Research Associateship Program.

Appendix A: The optical growth curve

Let $\mathcal{S}_n(X)$ be defined by

$$\mathcal{S}_n(X) = -2.5 \log_{10} \left[\frac{\int_0^{10(X-X_0)/n} x^{2n-1} \exp(-x) dx}{\int_0^\infty x^{2n-1} \exp(-x) dx} \right]$$

where X_0 is such as $\mathcal{S}_n(0) = 2.5 \log_{10}(2) = 0.75$.

According to Prugniel & Héraudeau (1998), $\mathcal{B}(X, T_p)$ is defined by:

$$\mathcal{B}(X, T_p) = \mathcal{S}_n(X), \quad n = (15 - T_p)/5$$

if $T_p < -5$ or $T_p > 10$ – corresponding to a Sérsic (1968) luminosity profile $i(A) \propto \exp[-(A/A_0)^{1/n}]$ –, and by

$$\mathcal{B}(X, T_p) = (2/3 - T_p/15)\mathcal{S}_4(X) + (1/3 + T_p/15)\mathcal{S}_1(X)$$

if $-5 < T_p < 10$, i.e., interpolated between the de Vaucouleurs profile and the exponential profile valid respectively for giant ellipticals and pure-disk galaxies.

Appendix B: Computation of NIR magnitudes and uncertainties

Let us first define $\mathcal{B}_i = \mathcal{B}(X_i, T_p)$,

$$S = \sum_{i=1}^n w_i,$$

where w_i is the weight attributed to the i^{th} point,

$$S_{\mathcal{B}} = \sum_{i=1}^n w_i \mathcal{B}_i,$$

$$S_{\mathcal{B}^2} = \sum_{i=1}^n w_i \mathcal{B}_i^2,$$

$$S_m = \sum_{i=1}^n w_i m_i,$$

$$S_{\mathcal{B}m} = \sum_{i=1}^n w_i \mathcal{B}_i m_i,$$

and

$$\Delta = S S_{\mathcal{B}^2} - S_{\mathcal{B}}^2.$$

Two methods have been used, depending essentially on the number of observations and their accuracy. In the first

one, the total NIR magnitude m_T is computed assuming $s = s_0$ by minimizing

$$\sum_{i=1}^n w_i (m_i - m_T - s_0 \mathcal{B}_i)^2$$

with respect to m_T . We obtain

$$m_T^{(1)} = (S_m - s_0 S_{\mathcal{B}})/S,$$

$$\sigma^2 [m_T^{(1)}] = \left(\sigma_{s_0}^2 S_{\mathcal{B}}^2 + \sum_{i=1}^n w_i^2 \sigma_i^2 \right) / S^2,$$

and the corresponding effective magnitude is

$$m_e^{(1)} = m_T + 2.5 \log_{10}(2)s_0,$$

$$\sigma^2 [m_e^{(1)}] = \left\{ \sigma_{s_0}^2 [2.5 \log_{10}(2)S - S_{\mathcal{B}}]^2 + \sum_{i=1}^n w_i^2 \sigma_i^2 \right\} / S^2.$$

We assume here that, for want of constraint on s , the uncertainty on s ($\sigma(s)$) is equal to the intrinsic scatter σ_{s_0} for this type.

In the second method, s is considered as a free parameter and m_T is computed by minimizing

$$\sum_{i=1}^n w_i (m_i - m_T - s \mathcal{B}_i)^2$$

with respect to m_T and s . We then get

$$m_T^{(2)} = (S_{\mathcal{B}^2} S_m - S_{\mathcal{B}} S_{\mathcal{B}m})/\Delta,$$

$$\sigma^2 [m_T^{(2)}] = \left[\sum_{i=1}^n w_i^2 \sigma_i^2 (S_{\mathcal{B}^2} - \mathcal{B}_i S_{\mathcal{B}})^2 \right] / \Delta^2,$$

$$s^{(2)} = (S S_{\mathcal{B}m} - S_{\mathcal{B}} S_m)/\Delta,$$

$$\sigma^2 [s^{(2)}] = \left[\sum_{i=1}^n w_i^2 \sigma_i^2 (S_{\mathcal{B}} - \mathcal{B}_i S)^2 \right] / \Delta^2,$$

$$m_e^{(2)} = m_T + 2.5 \log_{10}(2)s,$$

and

$$\sigma^2 [m_e^{(2)}] = \left\{ \sum_{i=1}^n w_i^2 \sigma_i^2 [S_{\mathcal{B}^2} - \mathcal{B}_i S_{\mathcal{B}} + 2.5 \log_{10}(2) (S \mathcal{B}_i - S_{\mathcal{B}})]^2 \right\} / \Delta^2.$$

Note that we have made the questionable assumption that the errors in the aperture magnitudes of a given galaxy are independent.

We are however not primarily interested in the best fitting growth curve, which would be determined assuming $w_i = 1/\sigma_i^2$, but rather in the best estimate of the asymptotic magnitude. When there is only one point, the

uncertainty on m_T is $\sigma(m_T) = (\sigma_1^2 + \mathcal{B}_1^2 \sigma(s)^2)^{1/2}$, i.e., the uncertainty on m_T decreases with the size of the aperture. It is therefore reasonable to adopt $w_i = 1/(\sigma_i^2 + \mathcal{B}_i^2 \sigma(s)^2)$ for all the points to give more weight to the large apertures.

To deal with outliers, we apply an iterative procedure. We initially assume $\sigma(s) = \sigma_{s_0}$ for the slope and $\sigma_i = \sigma_{m_0}$ for all the points. At each step, we fit the growth curve to the data, compute $\sigma(s)$ from above equations, and estimate new values of the uncertainties by $\sigma_i = \max(\sigma_{m_0}, |m_i - m_T - s\mathcal{B}_i|)$. This procedure is a compromise between our *a priori* uncertainty σ_{m_0} and the *a posteriori* estimate $[\sum_{i=1}^n (m_i - s\mathcal{B}_i)^2 / (n - k)]^{1/2}$, where $k = 1$ or 2 is the number of fitted parameters (and also the index of the method!). It has the advantage of reducing the weight of outliers and takes the scatter around the growth curve automatically into account. Practically, it improves the fit and gives a reasonable estimate of the uncertainties. The convergence is usually achieved in a few iterations.

The second method provides a better fit than the first one but is less secure because the slope of the growth curve is free. It is used only when following conditions are fulfilled simultaneously:

1. $n \geq 3$, which allows to check the validity of the fit,
2. $\sigma[m_T^{(2)}] < \sigma[m_T^{(1)}]$,
3. and

$$e^{-[s^{(2)} - s_0]^2 / [2\sigma_{s_0}^2]} \prod_{i=1}^n e^{-[m_i - m_T^{(2)} - s^{(2)}\mathcal{B}_i]^2 / [2\sigma_{m_0}^2]} \\ < \prod_{i=1}^n e^{-[m_i - m_T^{(1)} - s^{(1)}\mathcal{B}_i]^2 / [2\sigma_{m_0}^2]},$$

i.e., the fit provided by (2) is better enough than (1) to justify the deviation of s relatively to s_0 .

References

Aaronson M. 1977, Ph.D. thesis, Harvard University

Aaronson M., Huchra J., Mould J. 1979, ApJ 229, 1

Akritas M.G. 1999,
http://www.stat.psu.edu/~mga/scca/q_and_a/qa37.ps

Akritas M.G., Bershady M.A. 1996, ApJ 470, 706

Aparicio A. 1998, astro-ph/9811186

Baugh C.M., Cole S., Frenk C.S. 1996, MNRAS 283, 1361

Bernardi M., Renzini A., da Costa L.N., Wegner G., Alonso M.V., Pellegrini P.S., Ritte C., Willmer C.N.A. 1998, ApJ 508, L143

Bershady M.A. 1995, AJ 109, 87

Bessel M.S., Brett J.M. 1988, PASP 100, 1134

Boselli A., Gavazzi G. 1994, A&A 283, 12

Bottinelli L., Gougenheim L., Paturel G., de Vaucouleurs G. 1983, A&A 118, 4

Bower R.G., Lucey J.R., Ellis R.S. 1992, MNRAS 254, 601

Buta R. 1995, ApL&C 31, 109

Buta R., Mitra S., de Vaucouleurs G., Corwin H.G. 1994, AJ 107, 118

Christensen J.H. 1990, MNRAS 246, 535

de Jong R.S. 1996a, A&AS 118, 557

de Jong R.S. 1996b, A&A 313, 45

de Jong R.S. 1996c, A&A 313, 377

de Jong R.S., van der Kruit P.C. 1994, A&AS 106, 451

de Vaucouleurs G., de Vaucouleurs A., Corwin H.G., Buta R.J., Paturel G., Fouqué P. 1991, Third Reference Catalog of Bright Galaxies, Springer-Verlag

de Vaucouleurs G., de Vaucouleurs A., Corwin J.R. 1976, Second Reference Catalog of Bright Galaxies, University of Texas Press

de Vaucouleurs G., Corwin H.G. 1977, ApJS 33, 219

Faber S. 1973, ApJ 179, 731

Fioc M., Rocca-Volmerange B. 1997, A&A 326, 950

Frogel J.A., Persson S.E., Aaronson M., Matthews K. 1978, ApJ 220, 75

Gavazzi G. 1993, ApJ 419, 469

Gavazzi G., Boselli A. 1996, ApL&C 35, 1

Gavazzi G., Pierini D., Baffa C., Lisi F., Hunt L.K., Randone I., Boselli A. 1996a, A&AS 120, 521

Gavazzi G., Pierini D., Boselli A. 1996a, A&A 312, 397

Gezari D.Y., Pitts P.S., Schmitz M. 1997, Catalog of Infrared Observations, 4th edition, unpublished
http://iuewww.gsfc.nasa.gov/cio/cio_homepage.html

Griersmith D. 1980, AJ 85, 9

Hesselbjerg J. 1990, MNRAS 246, 535

Hubble E. 1926, ApJ 64, 321

Kauffmann G., Charlot S. 1998, MNRAS 29, 705

Kendall M.G., Stuart A. 1979, The Advanced Theory of Statistics, vol. 2, 4th edn, Charles Griffin, London

Kodaira K., Okamura S., Ichikawa S.-I. 1990, Photometric atlas of bright northern galaxies, University of Tokyo Press

Kodama T., Arimoto N., Barger A.J., Aragón-Salamanca A. 1997, A&A 320, 41

Larson R.B., Tinsley B.M., Caldwell C.N. 1980, ApJ 237, 692

Lin H., Kirshner R.P., Schechter P.L., Shectman S.A., Landy S.D., Oemler A., Tuckner D.L., Schechter P.L. 1996, ApJ 464, 60

Matthews W.G., Baker J.C. 1971, ApJ 170, 241

Mobasher B., Ellis R.S., Sharples R.M. 1986, MNRAS 223, 11

Paturel G., Andernach H., Bottinelli L., Di Nella H., Du rand N., Garnier R., Gougenheim L., Lanoix P., Marthinet M.C., Petit C., Rousseau J., Theureau G., Vauglin I., 1997, A&AS 124, 109

Peletier R.F., de Grijp R. 1998, MNRAS 300, L3

Press W.H., Teukolsky S.A., Vetterling W.T. and Flannery B.P. 1992, Numerical Recipes in Fortran: the Art of Scientific Computing, 2nd edition, Cambridge University Press

Prugniel Ph., Héraudeau Ph. 1998, A&AS 128, 299

Sandage A., Visvanathan N. 1978, ApJ 225, 742

Schade D., Carlberg R.G., Yee H.K.C., Lopez-Cruz O., Ellingson E. 1996, ApJL 464, L63

Schulte-Ladbeck R.E., Hopp U. 1998, AJ 116, 2886

Sérsic J.L. 1968, Atlas de galaxias australes, Observatorio Astronomico, Cordoba

Shioya Y., Bekki K. 1998, ApJ 504, 42

Terlevich R., Davies R.L., Faber S.M., Burstein D. 1980, MNRAS 196, 381

Tormen G., Burstein D. 1995, ApJS 96, 123

Tremblay B., Merritt D. 1996, AJ 111, 2243

Tully R.B., Pierce M.J., Huang J.-S., Saunders W., Verheijen M.A.W., Witchalls P.L. 1998, AJ 115, 2264